Geological Survey of Japan Cruise Report No. 20, p. 106–164, 1984

IX. LOCAL VARIABILITY OF MANGANESE NODULE DEPOSITS IN THE GH80–5 AREA

Akira Usui and Seizo Nakao

Introduction

Local variability of manganese nodule occurrence is important characteristic in understanding the nodule origin and in evaluating economic potential as metal resources. Significant small-scale (in the range of several kilometers) variations in abundance and bulk chemistry have been found in the abyssal hill area of the northeast equatorial manganese nodule belt (ANDREWS and FRIEDRICH, 1979; CRAIG, 1979; HALBACH and ÖZKARA, 1979). Such small-scale investigations have not been intensively made in the Central Pacific Basin. During the GH80–5 cruise, the 10 or 20 km grid survey including bottom sampling at each intersections and small-scale (one to two kilometer intervals) bottom sampling were made in two survey areas each extending 40×40 square kilometers. The purpose of this article is to characterize the pattern of small-scale variability of nodule deposits which should provide basic informations on the relationship between nodule growth process and geological conditions.

Methods

Nodule samplings were made using free-fall grabs (67 available operations), box cores (23), dredges (3) and piston corers (15). Nodules were found in 65 free-fall grabs, all of box cores, all of dredges and 11 piston cores. Nodule abundance is calculated from actually measured weights in the sampler and its sampling area (34×34 cm^2 for free-fall grabs, 40×40 cm^2 for box cores) by simple dividing. Sea floor coverage of nodules is estimated from the sea-bed photographs taken by 16 mm one-shot camera fixed to free-fall grabs and box cores by comparing the photos with standard color charts. Procedures of on-board sample description and observations were followed to those of our previous cruise GH80–1 (USUI, 1982). Available on-board nodule data are abundance, coverage, morphology, sea-bed occurrence, and size distribution. Chemistry (USUI and MOCHIZUKI, Chapter XV in this cruise report), mineralogy and internal structure (Usui, Chapter XIV in this cruise report) are summarized in other chapters.

Morphological classification

External morphology of manganese nodules has been described on board on the basis of surface feature, shape, and size (MEYLAN, 1974, MORITANI *et al.*, 1977). Surface feature has proved to be most available for nodule description and significant in relation to mineral composition (USUI, 1979). Nodules from the Central Pacific

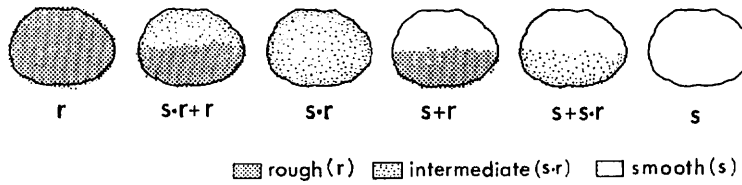

Fig. IX–1 Criteria of morphological type of manganese nodules based on surface feature.

Basin have been classified exclusively into types s(smooth surface) and r(rough surface) on board during earlier regional surveys of the GH cruises by G. S. J. Nodules of the GH80–5 cruises have, however, more variable and complex surface feature. They have sometimes intermediate surface (slightly rough: s·r) and features of tops and bottoms are often different. Therefore additional symbols such as s+r, s+s·r are defined during this cruise (Fig. IX–1). For instance, "s+s·r" means the nodule with top smooth surface(s) and bottom intermediate surface(s·r), and so on. The surface feature of nodules from a single sampler are generally similar, but nodules of slightly different surfaces (e.g., both s+r and s+s·r) occasionally occur in a single sampler.

Survey areas

Survey areas of this cruise lie in the northern part of the Central Pacific Basin which is terminated in the north by the Mid-Pacific Mountains. Figure IX–2 shows topography and manganese nodule data of the survey areas. In the south of the survey areas lies the Magellan Trough, an ancient axis of sea floor spreading (TAMAKI *et al.*, 1979). These areas are characterized by generally flat deep-sea basin with gently rolling abyssal knolls, and rugged topography in the vicinity of the Trough. Water depth ranges from 5500 to 6000 meters. Surface sediments are mostly recent siliceous fossil rich clays, and are underlain by pelagic and/or zeolitic clays (NISHIMURA, Chapter VII in this cruise report).

Two detailed survey areas, Area I (9°30′–10°10′N, 174°30′–174°50′W) and Area II (8°40′–9°20′N, 173°50′–174°10′W), were located so as to include several previous sampling stations. The Area I includes s-type nodules extensively distributed in the northern elevated area and r-type nodules in the southern deeper sea floor (GH76–1 cruise: MORITANI *et al.*, 1977). The Area II includes type s near the Magellan Trough and type r in the northern basin area (GH77–1 cruise: MORITANI *et al.*, 1979; GH80–1 cruise: USUI, 1982).

In the Areas I and II, continuous seismic reflection surveys were made on several parallel and crossing lines 10 km or 20 km apart. Nodules and bottom sediments were collected at each intersection as basic data of these areas. Detailed survey lines I–a, I–b, I–c, II–a and II–b were selected connecting two stations where nodule facies is characteristically different. The intervals of nodule sampling on these survey lines are one to two kilometers.

Local variation of nodule occurrence

These survey areas are characterized by high abundance of nodules. The probability of nodule presence on the sea floor calculated with all samplers is more than 94 per-

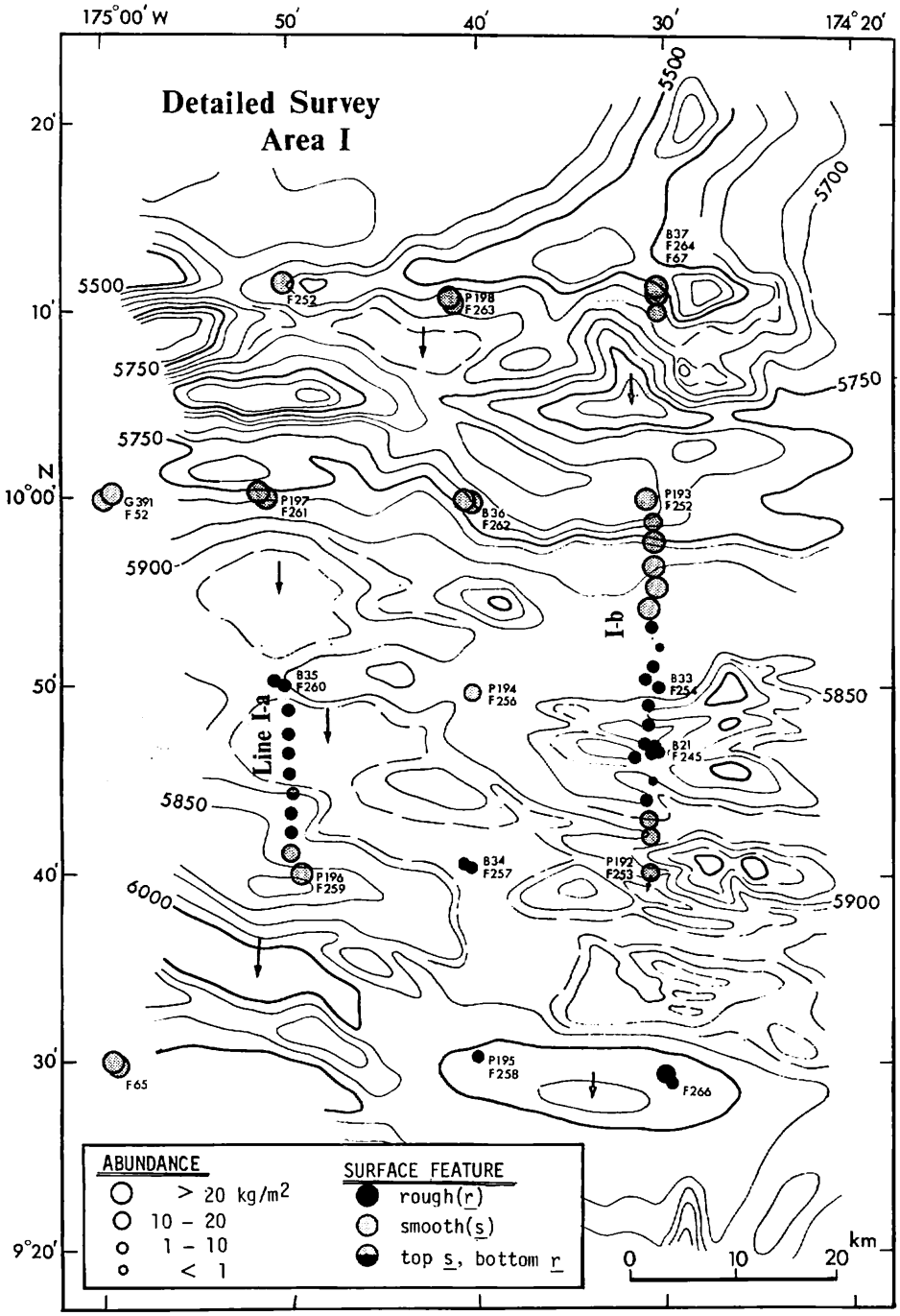

Fig. IX-2 (1)

Fig. IX-2(1, 2) Topography, sampling stations, nodule abundance and type. Previous data of GH76-1, GH77-1 and GH80-1 cruises are also plotted. Half solid symbol denotes the sample type s+r is present and the total of s+r and s+s·r exceeds 50 percent.

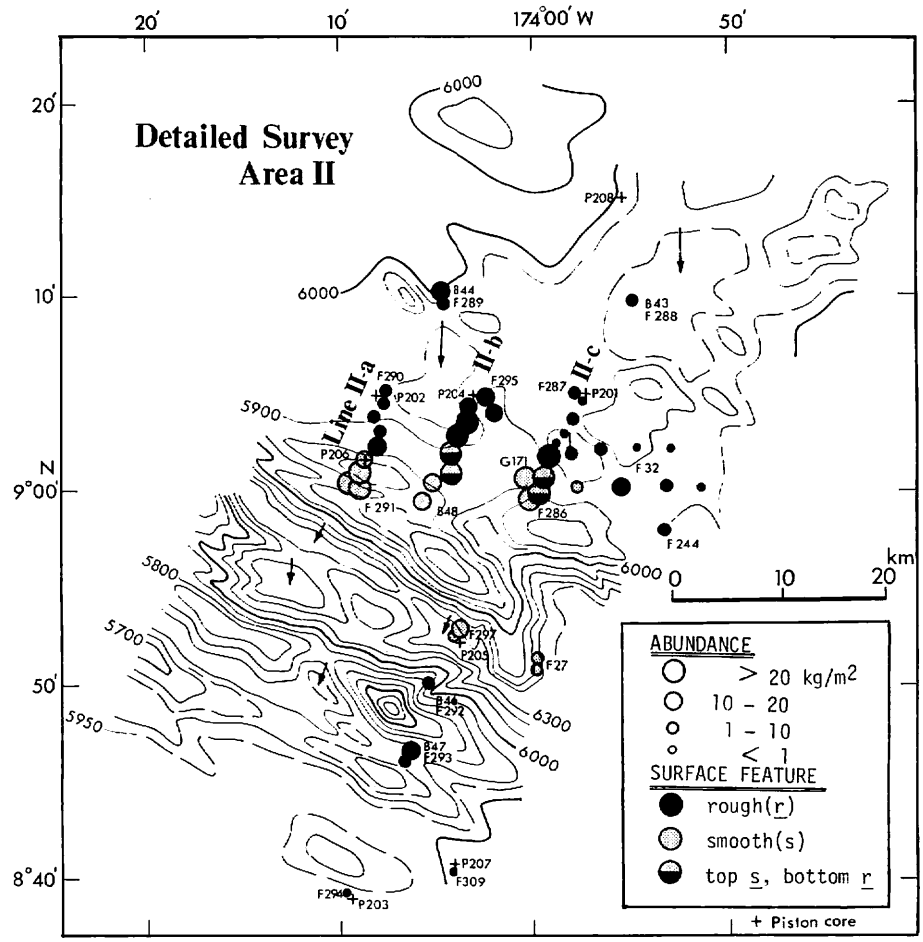

Fig. IX-2 (2)

cent in these areas. Abundance ranges from trace to more than 30 kg/m^2 and sea floor coverage from 0 to 80 percent. All of stationary data of manganese nodules are listed in Appendix IX–1 and photographs of samples and sea floor are shown in Appendix IX–2.

The plots of abundance and coverage (Fig. IX–3) and sea-bed photographs reveal somewhat difference in sea-bed occurrence of nodules from that of earlier regional observations in the Central Pacific Basin (MORITANI *et al.*, 1977; USUI, 1982). It has been pointed out that type r is completely buried within surface sediment and type s is exposed to sea water in general as summarized in Table IX–1. However, type r of the GH80–5 cruise is not always completely buried within surface sediment, but often discerned on the sea-bed photographs with thin sediment blanket on tops. This is especially the case when nodules are abundant (greater than ca. 5 kg/m^2) and/or the size is large (larger than ca. 4 cm in median value as shown in Table IX–2).

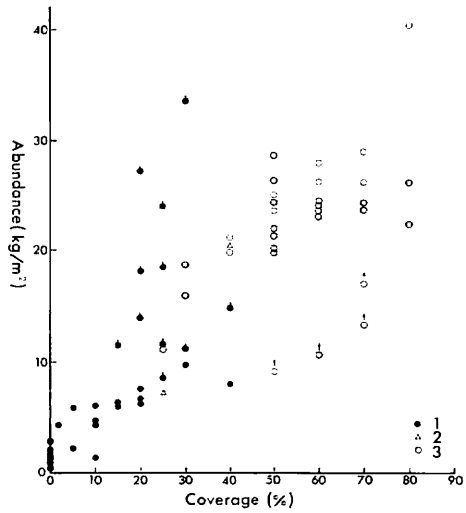

Fig. IX-3 Plots of nodule abundance versus coverage. Symbol 1 (solid circle) denotes type r and/or s·r+r dominant sample, 2 (triangle) type s+r and/or s·r dominant, 3 (open circle) type s and/or s+s·r dominant. Symbol 1 with a short bar on top means presence of s-type nodules inside. Symbol with an arrow mean possibility of underestimation of nodule abundance.

Table IX-1 Previous summary of manganese nodule characteristics in the Central Pacific Basin

Nodule type	r	s
Abundance	<10kg/m²	10-20kg/m²
Mode of size fraction	1-2cm	2-4cm
Occurrence on/in sediment surface	buried	exposed
Dominant shape	S, D	ID, IS, IDP
Internal structure	laminated, concentric, symmetrical	massive, compact, and surrounding thin layers
Internal cracks	rare	dominant
Polynucleation	rare	common
Dominant surface sediment associated	siliceous ooze or clay	zeolitic or pelagic clay

modified from Usui (1982)

In the Area I, type s (and minor s+s·r) dominates in the northern part (north of 10°N) and types s and r and intermediate types are found in the southern part (south of 10°N). The northern part is characterized by elevated and rugged topography. The nodule abundance is generally greater than 10 kg/m² and type s seem to be continuously distributed over this part. The southern part is typical deep-sea basin area with gently rolling hills and the water depth is deeper than 5800 m. Nodule distribution in the southern part is more complicated than in the northern part. The abundance of type s is greater than 10 kg/m² as well as in the northern part, while that of type r is less than 10 kg/m². Nodule type seem to vary from s to r on the scale of tens of kilometers and their distribution areas may be patchy.

On detailed survey line I–a (from 9°50′N–174°50′W to 9°40′N–174°50′W) and

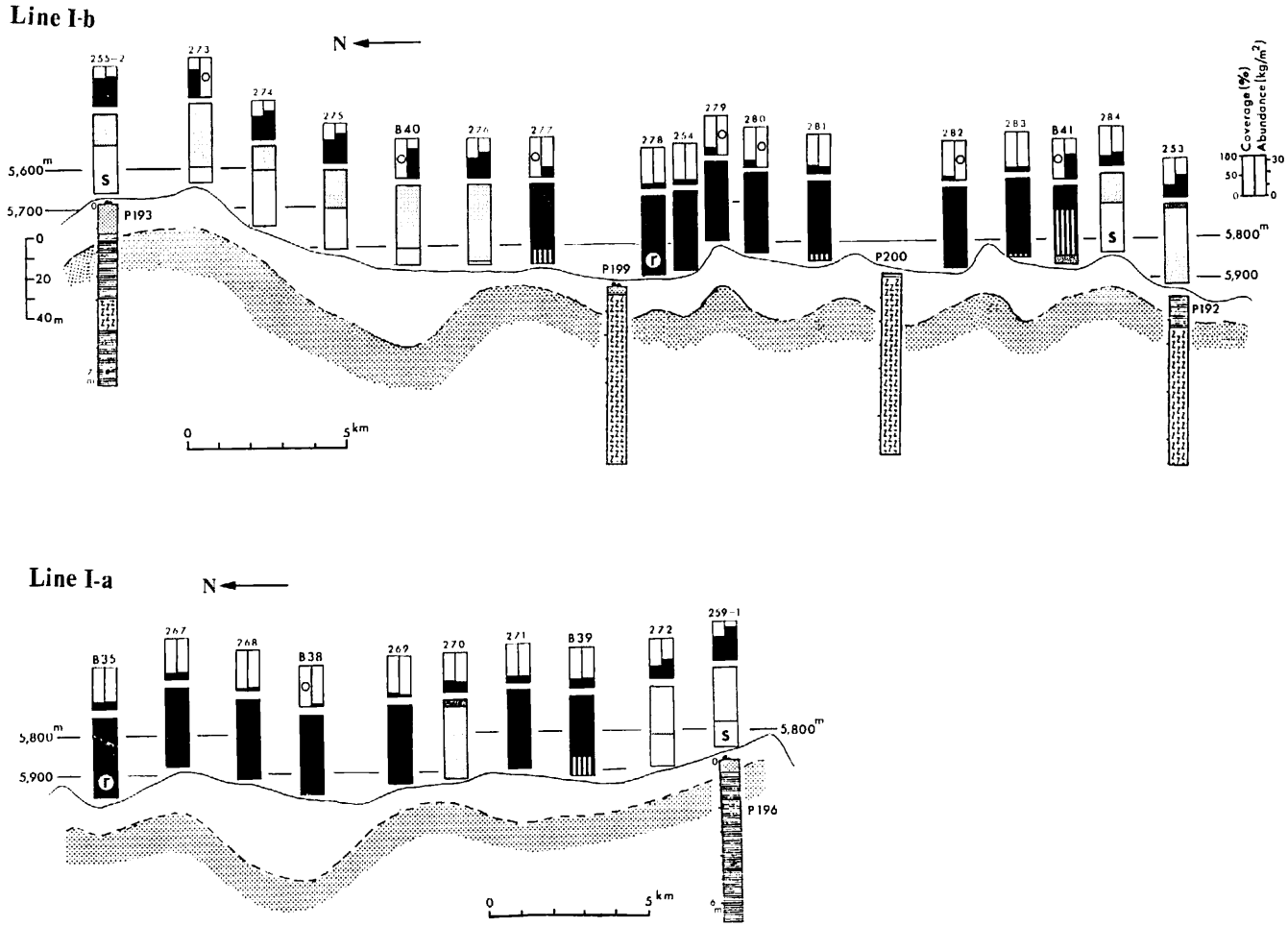
Line I-b
N
255-2
273
274
275
B40
276
277
278
254
279
280
281
282
283
B41
284
253
Coverage (%)
Abundance (kg/m²)
100
50
0
30
0
5,600m
5,700
S
P193
0
20
40m
P199
P200
P192
5,800m
5,900
0
5km
Line I-a
N
B35
267
268
B38
269
270
271
B39
272
259-1
5,800m
5,900
S
P196
0
5km

Fig. IX-4 (1)

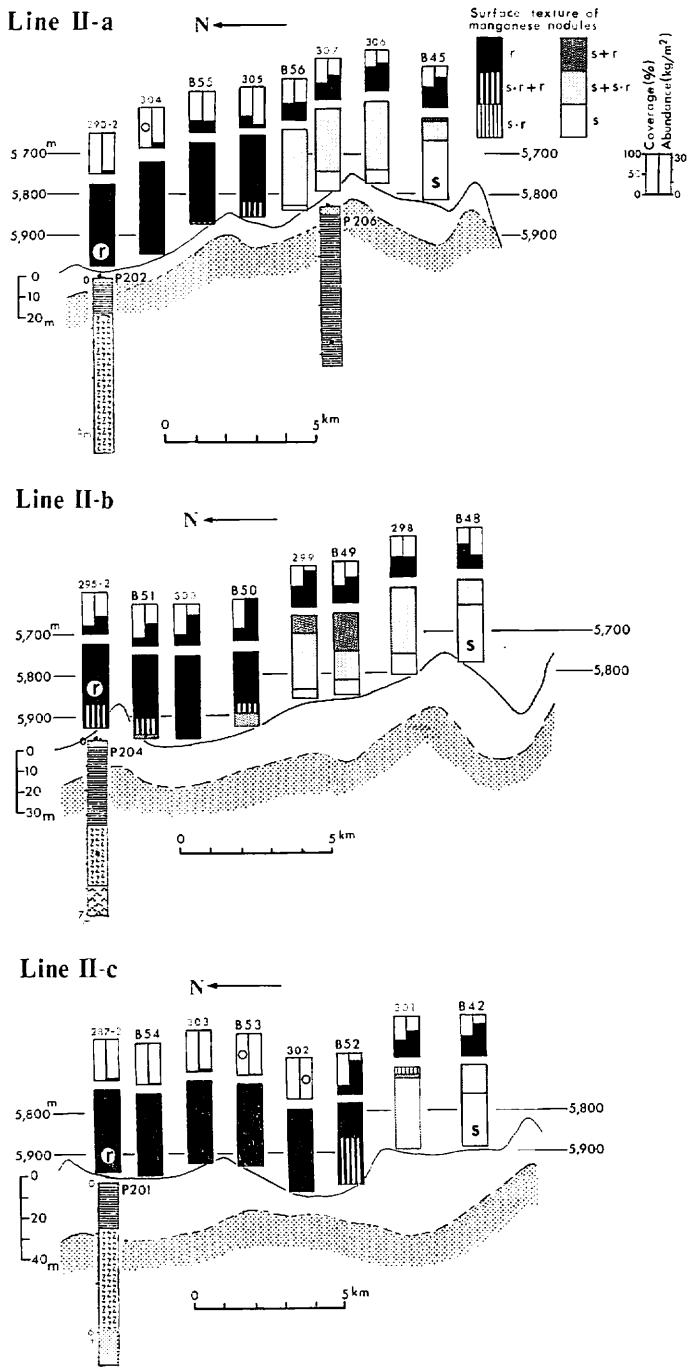

Fig. IX-4 (2)

Fig. IX-4(1–5) Local variation of nodule abundance and type on profiles of detailed survey lines. Shaded area in the profile is acoustically opaque basement on 3.5 kHz SBP records.

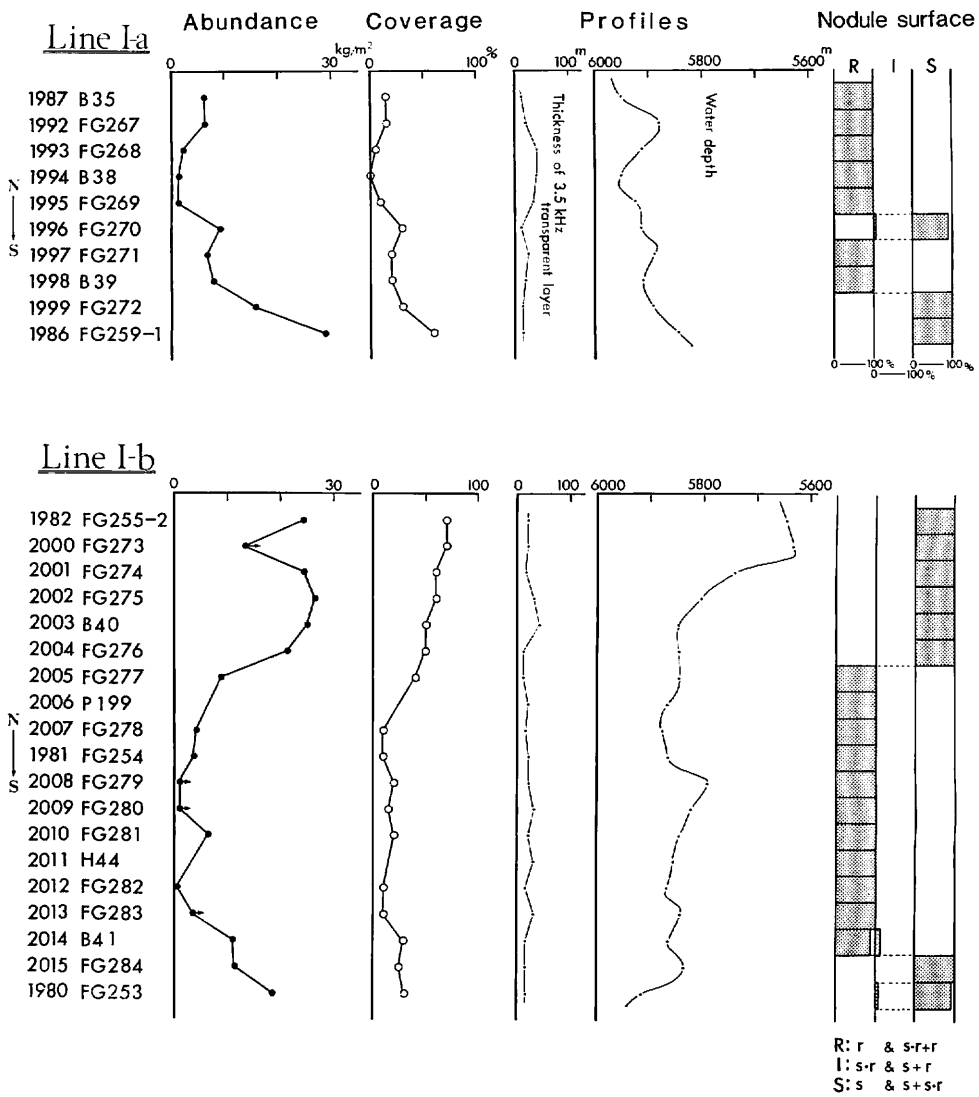

Fig. IX-5 (1)

Fig. IX-5(1-5) Summary of local variation of nodule facies and related geological factors on detailed survey lines. Numerical data are from Table IX-2.

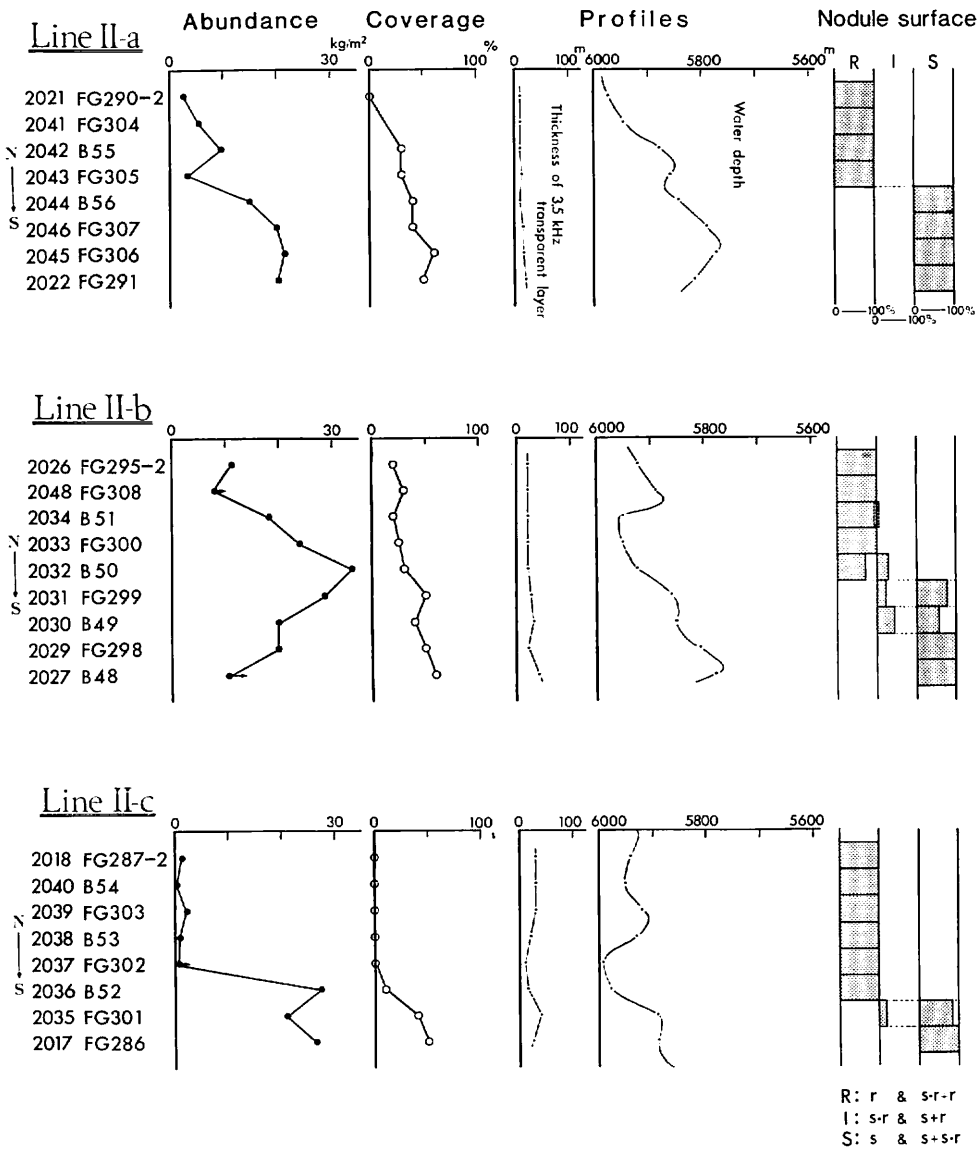
Line II-a
Abundance
Coverage
Profiles
Nodule surface
kg/m²
%
m
R I S
2021 FG290-2
2041 FG304
2042 B55
2043 FG305
2044 B56
2046 FG307
2045 FG306
2022 FG291
N
S
Thickness of 3.5 kHz transparent layer
Water depth
Line II-b
2026 FG295-2
2048 FG308
2034 B51
2033 FG300
2032 B50
2031 FG299
2030 B49
2029 FG298
2027 B48
Line II-c
2018 FG287-2
2040 B54
2039 FG303
2038 B53
2037 FG302
2036 B52
2035 FG301
2017 FG286
R: r & s-r-r
I: s-r & s+r
S: s & s+s-r

Fig. IX-5 (2)

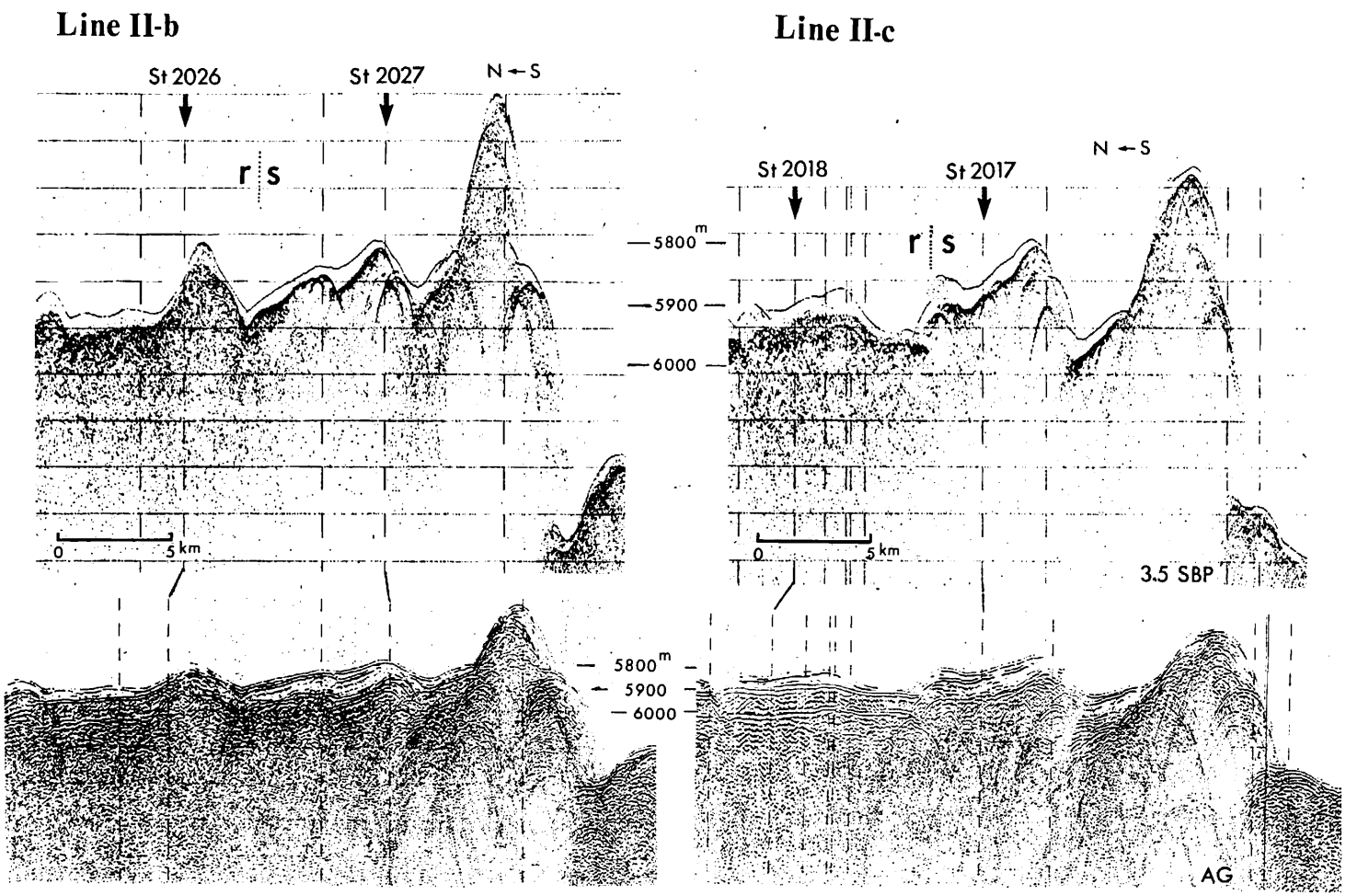

Fig. IX–6(1, 2) Seismic profiles of lines II–b and II–c by 3.5 kHz SBP and air gun.

Table IX-2 Local variation of manganese nodule characteristics.

Line no.	St./Sample no.		r	surface texture s•r+r	s•r	s+r	s+s•r	s	Shape	Abundance (kg/m²)	Coverage (%)	Size* (cm)	Polynucleation (no. %)
I-a	1987	B35	99	—	—	1	—	—	I, D, S	6.1	(15)	1.9	60
		FG260	100	—	—	—	—	—	S, D, SP	>3.4	—	2.5	30
	1992	FG267	100	—	—	—	—	—	S, SP	6.2	15	2.4	30
	1993	FG268	100	—	—	—	—	—	S	2.2	5	1.9	0
	1994	B38	100	—	—	—	—	—	S, D	1.5	(0)	2.3	10
	1995	FG269	100	—	—	—	—	—	S	1.3	10	2.0	20
	1996	FG270	—	—	—	6	94	—	I	9.2	30	3.8	40
	1997	FG271	100	—	—	—	—	—	S	6.6	20	2.8	50
	1998	B39	76	24	—	—	—	—	SP	2.6	(20)	3.1	60
	1999	FG272	—	—	—	—	58	42	IDP, ISP	15.9	30	3.5	40
	1986	P196	—	—	—	—	(100)	—	ID	—	—	—	—
		FG259-1	—	—	—	—	68	32	IDP	28.0	60	4.8(3.8)	50
I-b	1982	P193	—	—	—	—	(100)	—	ID	—	—	—	—
		FG255-2	—	—	—	—	39	61	IDP, ID	24.3	70	4.0(3.5)	30
	2000	FG273	—	—	—	—	82	18	IS, DP	13.3	70	3.8	20
	2001	FG274	—	—	—	—	31	69	IDP, DP	24.5	60	4.3	50
	2002	FG275	—	—	—	—	41	53	ID, DP	26.2	60	4.2	60
	2003	B40	—	—	—	—	80	20	IDP, ISP	25.1	(50)	4.3	30
	2004	FG276	—	—	—	—	95	5	SP, DP	21.4	50	4.7	70
	2005	FG277	82	18	—	—	—	—	SP, S, ISP	8.0	40	3.0	40
	2006	P199	(100)	—	—	—	—	—	S	—	—	—	—
	2007	FG278	100	—	—	—	—	—	S, D	4.4	10	2.3	20
	1981	B33	(100)	—	—	—	—	—	S, D	5.8	(5)	3.0	0
		FG254	100	—	—	—	—	—	S	3.8	10	2.4	0
	2008	FG279	100	—	—	—	—	—	S	>0.9	20	2.3	0
	2009	FG280	100	—	—	—	—	—	S	>0.9	15	2.8	0
	2010	FG281	90	10	—	—	—	—	S, D	6.4	20	2.1	20
	2011A	H44	(100)	—	—	—	—	—	S	—	—	—	—
	2012	FG282	100	—	—	—	—	—	S	0.2	10	1.7	0
	2013	FG283	96	4	—	—	—	—	S, D	>3.5	10	2.0	0
	2014	B41	29	61	—	10	—	—	D, S, IDP	11.3	(30)	3.7	70
	2015	FG284	—	—	—	—	36	64	I, ISP, IDP	11.5	25	2.9	80
	1980	FG253	—	—	—	4	96	—	I, IDP, ISP	18.7	30	4.0	70

II-a	2021	P202	(100)	—	—	—	—	—	S	—	—	—	—
		FG290-1	100	—	—	—	—	—	S, D	>0.7	0	3.0	0
		FG290-2	100	—	—	—	—	—	D, S	2.8	0	2.9	10
	2041	FG304	100	—	—	—	—	—	S, SP	5.4	—	3.8	40
	2042	B55	98	2	—	—	—	—	S, SP, D	9.7	30	3.8	40
	2043	FG305	80	20	—	—	—	—	D, ID	3.2	30	3.2	20
	2044	B56	94	6	—	—	—	—	ID, IDP, DP, D	14.8	40	5.1	50
	2046	P206	—	—	—	—	(100)	—	IDP	—	—	(5.0)	—
		FG307	—	—	—	—	77	23	IS, ID, IDP	20.0	40	5.1	50
	2045	FG306	—	—	—	—	83	17	ID, DP, IS	23.1	60	4.4	40
	2022	B45	—	—	—	3	26	71	ID, I	24.4	50	4.9	30
		FG291	—	—	—	—	10	90	ID, IS, F	20.5	50	3.5	40
II-b	2026	FG295-1	91	9	—	—	—	—	IDP, D, ISP, S	11.3	25	5.0	10
		FG295-2	71	29	—	—	—	—	ISP, IDP	13.9	20	5.0	40
		P204	(100)	—	—	—	—	—	SP	—	—	—	—
	2048	FG308	100	—	—	—	—	—	IS, SE	>8.1	30	5.8	0
	2034	B51	75	20	—	5	—	—	ID, IDP	18.1	20	5.4	10
	2033	FG300	100	—	—	—	—	—	S, SE, IS	24.0	25	7.3	0
	2032	B50	60	12	—	28	—	—	IS, ISP, ID	33.6	30	6.8	10
	2031	FG299	—	—	—	22	67	11	IS, ID	28.6	50	6.7	30
	2030	B49	—	—	—	45	37	18	ID, IS, IDP	20.2	40	4.3	20
	2029	FG298	—	—	—	—	75	25	ID, IS, IDP	19.9	50	4.2	50
	2027	FG296	—	—	—	—	—	(100)	F(crust?)	1.7	(30)	(4.0)	0
		B48	—	—	—	—	29	71	ID, IS, IDP	10.6	60	4.4	30
II-c	2018	P201	—	—	—	—	—	—	—	0	—	—	—
		FG287-1	100	—	—	—	—	—	D, IS	1.3	—	1.8	10
		FG287-2	100	—	—	—	—	—	IS, I, S	1.0	0	2.7	30
	2040	B54	100	—	—	—	—	—	S, I	0.3	0	1.5	0
	2039	FG303	100	—	—	—	—	—	S, I	2.1	0	1.6	0
	2038	B53	100	—	—	—	—	—	S, D	0.8	(0)	1.7	0
	2037	FG302	100	—	—	—	—	—	S	>0.6	0	2.0	0
	2036	B52	43	57	—	—	—	—	S, SE	27.3	20	9.2	0
	2035	FG301	—	—	9	4	87	—	IS, ID, F	21.1	40	5.0	10
	2017	FG286	—	—	—	17	66	17	IS, ID	26.5	50	7.8	10
		B42	—	—	—	—	35	65	IS, DP, IDP	23.6	(50)	5.1	20

* median of long axis

line I–b (from 10°00′N–174°30′W to 9°40′N–174°30′W), significant variations of nodule abundance and morphology were found. The boundary of two characteristic types s and r on the two survey lines seems considerably sharp. In the boundary area, nodules usually have different tops and bottoms in surface feature, e.g., s+s·r, s+r, s·r+r (Table IX–2, Fig. IX–4 and Fig. IX–5).

In the Area II, three detailed survey lines II–a, II–b and II–c were situated normal to the axis of the Magellan Trough (Fig. IX–3B). Mode of distribution of nodules along these three lines are similar to each other. It seems with these detailed line surveys that the Area II distribution pattern of types s to r are concordant to the topographic trend of NWW-SEE. They cover s- and r-type nodule areas from the Magellan Trough to northern basin area.

Type s is distributed in the crest and flank of the northern ridge and in the floor of the Magellan Trough. The abundance of type s usually exceed 20 kg/m^2, and the coverage is greater than 50%. On the other hand, type r is distributed in the flat basin areas north off the Trough. The abundance is generally less than 10 kg/m^2, though in the transitional zone of types s to r anomalously great abundance of type r (more than ca. 20 kg/m^2) is encountered at St. 2044–B56 of I–a, St. 2033–FG300 of I–b, and St. 2036–B52 of I–c. This anomalous r-type nodules always contain older s-type nodules inside and entirely coated with outermost rough layers (USUI, Chapter XIV in this cruise report). In contrast, r-type nodules from the basin areas contain no s-type nodules inside, but are entirely composed of typical rough layers. The abundance rarely exceeds 5 kg/m^2 in this case. Thus, the great nodule abundances (more than 10 kg/m^2) encountered in these areas is mainly attributed to the dominant older type-s nodules inside.

Significant local variations of nodule facies were, as mentioned, observed in the Areas I and II. It has been an important scientific and economical problem to correlate the mode of regional and local variations to any geological factors. However, no prominent factors generally applicable have been found. In these areas, the mode of variation of nodule facies were precisely compared with several geological parameters such as water depth, topography, thickness of transparent layer, surface sediment type. But the variations could not be simply correlated to either of them. A weak correlation between the nodule type and topography could be observed. Type s is likely to occur in the topographic highs on the scale of hundreds of meters, such as in the northern elevated part of Area I and in the northern ridge of the Magellan Trough of Area II. However, type s is sometimes found in the flat basin area, such as in the line I–b (Fig. IX–4A).

A small scale undulation of deep-sea basin characterized by abyssal knolls in the range of tens of meters is not related to the variations of nodule abundance or type (Fig. IX–5).

Surface sediment of the two detailed survey areas are mostly siliceous fossil rich clay (NISHIMURA, Chapter VII in this cruise report). No distinct difference of surface sediment type is observed along any detailed survey lines, although nodule facies is greatly variable.

Uppermost acoustically transparent layer, which have been correlated to Quaternary to Eocene unconsolidated sediments in the northern Central Pacific Basin (TAMAKI *et*

al., 1977), are ubiquitously distributed in these survey areas. Thickness of these transparent layers is small and uniform as compared with those observed during earlier works. The thickness ranges from 10 to 50 meters on the detailed survey lines (Fig. IX–5). The variation of nodule abundance or type seem to have no relationship to the thickness of the uppermost transparent layer, which does not agree with earlier observation by MIZUNO *et al.* (1981). Only an apparent relationship is the sharpness of the reflector between the transparent layer and underlying opaque layers in 3.5 kHz SBP records (Fig. IX–6), which may suggest a substantial difference of the opaque layer and a relationship of past sedimentary condition to nodule forming processes.

Buried Nodules

Manganese nodules occur within piston cores some of which reach the late Eocene sediments (NISHIMURA, Chapter VII in this cruise report). Nodules were found at ten horizons from seven piston cores, P193, P197, P198, P203, P204, P205 and P206 (Appendix IX–3). Buried nodules are of entirely smooth surface (type s) except for one nodule of indefinite surface from P203. Most of buried nodules are associated with pelagic clay of late Pliocene to late Pleistocene (NISHIMURA, Chapter VII in this cruise report). Nodules are scarce within underlain zeolitic clays, though one nodule was found from P204. The relationship between piston core stratigraphy (NISHIMURA, Chapter VII in this cruise report; JOSHIMA, Chapter X in this cruise report) and buried nodule occurrence suggests that they are diversely distributed in various horizons from late Pliocene to Recent. The horizons of buried nodules are not exactly correlated to each other cores. Only a few correlations are possible between P173, P197, P198 and P206.

These core stratigraphy and sedimentation rate also show no clear evidence that nodules lie in the horizon of erosion of sediments and/or lack of sedimentation (hiatus).

Summary

Small-scale grid and line surveys have revealed significant local variations in nodule abundance and type. The surface feature varies from smooth to rough, and within transition zones the nodules of different top and bottom surface features are common. Abundance of type s is generally greater than 10 kg/m^2, while type r is less. As nodule type varies from type s to type r, abundance decreases from 20 kg/m^2 to traceable, with considerably drastic decrease in the boundary zones. Anomalously great abundance of type r is encountered locally in boundary zones from type s to r in the Area II, which is attributable to dominant older s-type nodules inside the type r.

Sea-bed occurrence of type s and r observed during earlier surveys in the Central Pacific Basin, that is, type r is completely buried within surface sediments and invisible on sea-bed photos, was not always confirmed in these Areas I and II. Typical rough nodules were often observed on the sea-bed photos usually with a thin sediment blanket on tops.

The pattern of variation of nodule abundance and morphological type was compared with several geological factors along the detailed survey lines. Water depth ranging from 5500 to 6000 m and surface sediment (siliceous fossil rich clay through-

out these areas) seem to have no relationship to nodule abundance or type. Only a slight control of nodule facies is that type s of high abundance is likely to occur in the topographic highs while type r is in the deeper basin areas, though exceptional cases are also encountered. Thickness of uppermost transparent layers in seismic profiles is considerably uniform but no concordant variation with nodule facies is recognized. Sharpness of reflector between the uppermost transparent layer and underlain opaque layer in the 3.5 kHz SBP records appear to be related to nodule type only in the survey lines II–b and II–c. Sediment lithology and stratigraphy established for piston cores may be related to nodule facies. Though surface sediment are siliceous fossil rich clay, underlain sediments are variable. The area of type r may be correlated to thin siliceous fossil rich clay surface sediment and underlain zeolitic clay. The sedimentary history of the associated sediments would be the most probable factor to be related to the nodule forming processes.

References

ANDREWS, J. E. and FRIEDRICH, H. W. (1979) Distribution patterns of manganese nodule deposits in the Northeast Equatorial Pacific. *Marine Mining*, vol. 2, no. 1/2, p. 1–43.

CRAIG, J. D. (1979) Geological investigation of the Equatorial North Pacific sea-floor: a discussion of sediment redistribution. *In* BISCHOFF, J. L. and PIPER, D. Z. (*eds.*) *Marine Geology and Oceanography of the Pacific Manganese Nodule Province*, Marine Sci. Ser., Plenum Publ. Co., vol. 9, p. 529–557.

HALBACH, P. and ÖZKARA, M. (1979) Morphological and geochemical classification of deep-sea ferromanganese nodules and its genetical interpretation. *In* LALOU, C. (*ed.*) *La Genèse des Nodules de Manganèse*. C. N. R. S. Rept. no. 289, p. 77–88.

MEYLAN, M. A. (1974) Field description and classification of manganese nodules. *Hawaii Inst. Geophys. Rep.*, HIG–74–9, p. 158–168.

MIZUNO, A. (1981) Regional and local variabilities of manganese nodules in the Central Pacific. *Geol. Surv. Japan Cruise Report*, no. 15, p. 281–296.

MORITANI, M., MARUYAMA, S., NOHARA, M., KINOSHITA, Y., OGITSU, T., and MORIWAKI, H. (1977) Description, classification, and distribution of manganese nodules. *Geol. Surv. Japan Cruise Report*, no. 8, p. 136–158.

MORITANI, M., MARUYAMA, S., NOHARA, M., KINOSHITA, Y., KOIZUMI, T., and ITO, T. (1979) Description, types and distribution of manganese nodules. *Geol. Surv. Japan Cruise Report*, no. 12, p. 163–205.

TAMAKI, K. (1977) Study on substrate stratigraphy and structure by continuous seismic reflection profiling survey. *Geol. Surv. Japan Cruise Report*, no. 8, p. 51–62.

TAMAKI, K., JOSHIMA, M., and LARSON, R. L. (1979) Remanent Early Cretaceous spreading center in the Central Pacific Basin. *J. Geophys. Res.*, vol. 84, p. 4501–4510.

USUI, A. (1979) Minerals, metal contents and mechanism of formation of manganese nodules from the Central Pacific Basin (GH76–1 and GH77–1 areas). *In*

BISCHOFF, J. L. and PIPER, D. Z. (*eds.*) *Marine Geology and Oceanography of the Pacific Manganese Nodule Province*, Marine Sci. Ser., Plenum Publ. Co., vol. 9, p. 651–679.

USUI, A. (1982) Variability of manganese nodule deposits: the Wake-Tahiti transect. *Geol. Surv. Japan Cruise Report*, no. 18, p. 138–223.

Appendix IX-1 Sample list and results of on-site

Station/Sample No.		Sea-bed photograph: Nodule coverage (%)	Sea-bed photograph: Sediment consistency	Sediment type	Morphological type	Manganese: Abundance (kg/m²)	Manganese: Size distribution (long axis) >10	10-8	8-6	6-4	4-2	2-1	<1cm
1979	FG252-1	80		sfrC	ISs, IDPs	40.3		2	14	21	34		
	-2	80		sfrC	ISs, IDs	(10.6)			2	6	10		
1980	P192	—		—	—	—							
	FG253	30	H′	sC	IDPs+s·r, Ts+r, Ds+s·r	18.7	2	1	3	20	24	2	
1981	B33	(5)		pC	Sr, Dr	5.8				3	14	2	1
	FG254	10		pC	Sr, Dr	3.8				4	18	11	4
1982	P193	—		sC	IDs+s·r	—				1			
	FG255-1	70	H′	sfrC	IDPs, Ds	(16.9)				31	59	1	
	-2	70	H′	sfrC	IDPs, Ds	24.3			2	10	12		
1983	P194	—		sfrC	Ds·r	—					1		
	FG256-1	50		sfrC	DPs+s·r, ISs+s·r, Ds+s·r	21.8		1	1	25	23		
	-2	40		sfrC	Is+r, Ds+s·r, IDPs+s·r	19.2	2	4		14	25		
1984	B34	(10)		sfrC	Sr, SPr	4.7				7	30	48	3
	FG257	20		sfrC	Sr, SPr	7.6				5	28	35	
1985	P195	—		sfrC	Sr, SPr	—				1	3		
	FG258-1	10		sfrC	Sr, SPr	3.2				4	10	4	1
1986	P196	—		sfrC	IDs+s·r	—					2		
	FG259-1	60	H′	sfrC	IDPs+s·r, DPs	28.0			9	31	14		
	-2	60	H′	sfrC	IDPs+s·r, DPs	(10.0)				10	12		
1987	B35	(15)		pC	Ir, Dr, Sr, Ts+r	6.1			1	9	36	52	2
	FG260	—		sfrC	Sr, Dr, SPr, Ir	(3.4)			1	3	11	9	
1988	P197	—		sfrC	IDPs+s·r	—					1		
	FG261-1	70	H′	sfrC	ISs, DPs, IDPs, Fs	26.1				22	37		
	-2	70	H′	sfrC	ISs, DPs, IDPs, Fs	23.7				30	85		
1989	B36	(60)		sfrC	ISs, DPs, IDPs, Fs	24.1			4	40	76	2	
	FG262	70		sfrC	ISs, DPs, IDPs, Fs	28.9			1	25	50		
1990	P198	—	—	sfrC	IDs+s·r	—				(3)			
	FG263-1	80	H′	sfrC	IDs+s·r, DPs, Ds	22.4			1	16	29		
	-2	80		sfrC	IDs+s·r, DPs, Ds	26.2			3	17	55	2	

observation of manganese nodules and associated data.

nodules					
Total weight (g)	Position on/in sediment	Internal structure	Nucleus	Polynucleation (%)	Associated material
4660		irregular nodule fragments and surrounding layers	zeolite/clay	0	
1220		do.	shark tooth	0	
0				—	
2166		coalescent small nodules on top, concentric bands	zeolite/clay	70	
526	completely buried			0	pumice, micronodules
442		concentric bands	small brown particle	0	
101	1 nodule (-705)			—	
1956		irregular nodule fragments and surrounding layers		20	
2812				30	
25				—	
2520		irregular nodule fragments and 2mm surrounding layers		60	
2225		do.	irregular rock (zeolite?)	40	zeolitic rock (?)
710	most buried, large nodules exposed			30	shark teeth, pumice, micronodules
873		concentric bands		30	zeolitic rock (?)
48				(20)	
370		concentric bands	brown particle	30	
51				—	
3240		irregular nodule fragments and surrounding layers		50	
1225				50	
922	most exposed, some buried	irregular nodule fragments and surrounding layers	irregular brownish clastics	60	shark teeth, zeolitic rock(?), micronodules
398		do.	small brown particle	30	
24	1 nodule (-173) 1 nodule (-636) 2 nodules (-685)			—	
3015		irregular nodule fragments and surrounding layers	zeolite/chert	70	
2735		do.		60	
3660	exposed	do.	small brown particle	30	benthic foraminifera
3339				30	
114	1 nodule (-473) 3 nodules (-718)			—	
2584		irregular nodule fragments and surrounding layers	zeolite	30	
3026		do.		20	

Station/Sample No.		Sea-bed photograph: Nodule coverage (%)	Sea-bed photograph: Sediment consistency	Sediment type	Morphological type	Manganese: Abundance (kg/m²)	Manganese: Size distribution (long axis) >10	10-8	8-6	6-4	4-2	2-1	<1cm
1991	B37	(70)		sC	DPs, IDPs, ISs	26.2			2	41	74	10	
	FG264	70	H	sfrC	ISs, DPs, Ds	17.0				17	36		
1992	FG267	15		sfrC	Sr, SPr, Dr	6.2		1	1	4	39	25	3
1993	FG268	5	L	sfrC	Sr, Dr	2.2				2	8	10	2
1994	B38	(0)		sfrC	Dr, Sr	1.5				2	6	3	3
1995	FG269	10	L	pC	Sr	1.3					9	7	2
1996	FG270	30	M	sfrC	ISPs+s·r	9.2			5	18	26	3	
1997	FG271	20	L	sfrC	Sr, SPr, Dr	6.6			1	3	38	11	1
1998	B39	(20)		sfrC	SPs·r+r, Ds·r+r, Dr	7.6				27	34	20	3
1999	FG272	30	M	sfrC	IDPs+s·r, ISPs+s·r	15.9			2	25	58		
2000	FG273	70	H′	—	ISs+s·r, DPs+s·r, Ds	13.3			3	14	20	1	1
2001	FG274	60	H′	sfrC	IDPs+s·r, DPs, ISs	24.5			3	25	20		
2002	FG275	60		sfrC	IDs+s·r, DPs+s·r, ISs	26.2			4	24	24		
2003	B40	(50)		sfrC	ISPs+s·r, IDPs+s·r	25.1			5	41	32		
2004	FG276	50		sfrC	SPs+s·r, DPs+s·r, ISPs+s·r	21.4		1	7	39	18		
2005	FG277	40	M	sfrC	SPs·r+r, Sr, Ds·r+r	8.0				14	27	14	
2006	P199	—		sfrC	Sr	—						2	
2007	FG278	10		sfrC	Sr, Dr	4.4				3	34	21	5
2008	FG279	20	L	sfrC	Dr, Sr	(0.9)					6	4	
2009	FG280	15	L	—	Sr	(0.9)					6	1	
2010	FG281	20	L	sfrC	Sr, Dr, SPr	6.4				2	51	40	6
2011	P200	—		sfrC		(0)							
2011A	H44	—		sfrC	Sr	—						1	
	FG285	30	M	—	Ds·r+r, DPs·r+r	2.7				2	15		
2012	FG282	10	L	—	Sr	(0.2)					1	3	
2013	FG283	10	L	zrC	Sr, Dr, SPr	3.5				1	25	28	
2014	B41	(30)		sfrC	Ds·r+r, Sr, IDPs·r+r	11.3			5	26	34	8	
2015	FG284	25	M	—	IDPs, ISs, IDPs+s·r	11.5	1	1	2	8	47	16	1
2016	D463	—		—	Dr, Sr, Ir	—				—	—		
2017	B42	(50)		sfrC	ISs+s·r, DPs+s·r, Ds	23.6		2	14	29	13		
	FG286	50	H′	sfrC	ISs+s·r, IDs+s·r	26.5		12	11	3			

(continued)

nodules					
Total weight (g)	Position on/in sediment	Internal structure	Nucleus	Polynucleation (%)	Associated material
3979	exposed	do.		20	benthic foraminifera
1960				30	
721		concentric bands	small brown rock	30	shark teeth
257		internal compact nodule, surrounding concentric bands		0	
233	most buried, few exposed	do.	zeolite (?)	10	micronodules, pumice, benthic foraminifera
152		concentric bands		20	
1067		2–3cm thick layers surrounding irregular rocks	zeolite	40	
766		concentric bands		50	
1150	most buried	do.		60	shark teeth, zeolite(?), benthic foraminifera
1840		internal compact nodules, surrounding concentric bands	zeolite (?)	40	benthic foraminifera
1535		irregular nodule fragment, surrounding layers		20	
2827		do.		50	
3025		do.		60	
3811	most exposed (partly buried)	do.		30	
2475		internal compact nodules, surrounding layers		70	
923		concentric bands, with internal cracks	zeolite	40	shark teeth
11				—	
510		concentric bands	zeolite (?)	20	
99		do.		0	
102		do.		0	
737		do.		20	
0				—	
7				(0)	
317		concentric bands, some case internal nodule fragments	zeolite	50	pumice
23		concentric bands		(0)	
410		do.		0	
1716		small nodules concentric, large ones internal nodule fragments	shark teeth, zeolite	70	shark teeth
1328		irregular nodule fragments, surrounding layers		80	
~33kg				—	shark teeth, pumice
3586	exposed	irregular nodule fragments, surrounding layers		20	pumice
3064		do.		10	

Station/Sample No.		Sea-bed photograph: Nodule coverage (%)	Sea-bed photograph: Sediment consistency	Sediment type	Manganese: Morphological type	Manganese: Abundance (kg/m²)	Manganese: Size distribution (long axis): >10	10–8	8–6	6–4	4–2	2–1	<1 cm
2018	P201	—		sfrC	—	—							
	FG287-1	—	L	sfrC	Dr, Ir, Sr	1.3				1	7	10	2
	-2	0		sfrC	ISr, Ir, Sr	1.0				1	6	3	
2019	B43	0	M	sfrC	Dr, Sr	1.7				3	3	1	
	FG288	—		sfrC	—	0							
2020	B44	25	M	sfrC	IDPr	18.6		2	11	8	10		
	FG289	25	M	—	Dr, IDPr, SEr	7.4			3	6	6		
2021	P202	—		sC	Sr	—					1		
	FG290-1	0	L	sfrC	Sr, Dr	(0.7)					3		
	-2	0		sfrC	Dr, Sr	2.8				3	7	4	
2022	B45	50	H′	sfrC	IDs+s·r, ISs+s·r, IDs	24.4		1	24	25	27	1	
	FG291	50	H′	sfrC	IDPs+s·r, ISs+s·r, Fs	20.5				16	35		
2023	B46	(30)		sfrC									
	FG292	2	L	sfrC	IDPr, ISr	4.3				10	10	1	
2024	B47	25	M	sfrC	IDPr	8.7			6	15	9		
	FG293	15	L	sfrC	IDPr	11.5			4	10	11		
2025	P203	—		pC	—	(0)							
	FG294-1	0		sfrC	—	0							
	-2	—		sfrC	Dr, Ir	0.1						6	4
2026	P204	—		sfrC	SPr	—					1		
	FG295-1	25		—	IDPr, Dr, ISPr, Sr	11.3		2	2	6	4		
	-2	20	M	sfrC	ISPr, IDPr, Dr	13.9		4	3	13	7		
2027	B48	60		sfrC	IDs, ISs, IDPs, IDs+s·r	10.6			1	37	22	1	
	FG296	(30)	M	—	Fs	(1.7)				1	1		
2028	P205	—		sfrC	ISs, ISs+s·r	—				2			
	FG297-1	50	H′	sfrC	ISs, IDs	9.2			3	7	10		
	-2	60	H′	sfrC	IDs, IDPs, DPs, Fs	23.6			1	18	87		
2029	FG298	50		sfrC	IDs+s·r, ISs+s·r, IDPs+s·r	19.9			1	17	15		
2030	B49	40		sfrC	IDs+r, ISs+r, IDPs+r	20.2		1	11	19	25		
2031	FG299	50	M	sfrC	ISs+s·r, IDs+s·r, IDs	28.6		8	20	15			
2032	B50	30		sfrC	ISr, ISPr, IDr	33.6		5	14	5	3		

(continued)

nodules

Total weight (g)	Position on/in sediment	Internal structure	Nucleus	Polynucleation (%)	Associated material
0				—	
150		concentric bands	pumice/clay	10	
120		do.	do.	30	
253	completely buried	internal compact nodule, surrounding layers (~1cm)	brownish rock	30	
0					
2830	most buried, large nodules exposed	internal compact nodule, surrounding layers (~1cm)	brownish rock	70	pumice, whale ear bone (?)
854		do.		50	pumice
17				—	
78		internal compact nodule, surrounding layers		0	pumice
322				10	
3713	exposed	surrounding layers of nuclei or nodule fragments	zeolite (?)	30	pumice
2370		do.	zeolite (?), shark teeth	40	
492		irregular nodule fragments, surrounding layers	zeolitic rock (?)	40	pumice, zeolitic rock (?)
1240	(buried)	do.		70	
1333				30	
0	1 nodule (-276)				
0		concentric bands	pumice (?)		
14				0	
15	1 nodule (-460)			(0)	
1306		internal compact nodule, surrounding layers (~1cm)	zeolite	10	
1610		do.		40	
1616	exposed	irregular nodule fragments, surrounding layers		30	
192				0	zeolitic rock (?)
170	1 nodule (-241)			0	
1064		irregular nodule fragments, surrounding layers		20	
2732				20	
2302		irregular nodule fragments, surrounding layers	zeolite	50	
3075	exposed (half buried)	do.	do.	20	pumice
3305		do.	do.	30	
5115	partly exposed	compact and fractured nodules inside, surrounding layers (~1cm)		10	shark teeth

Station/Sample No.		Sea-bed photograph: Nodule coverage (%)	Sea-bed photograph: Sediment consistency	Sediment type	Morphological type	Manganese: Abundance (kg/m²)	Manganese: Size distribution (long axis) >10	10-8	8-6	6-4	4-2	2-1	<1cm
2033	FG300	25	L	sfrC	Sr, SEr, ISr	24.0		3	8			1	
2034	B51	20	M	sfrC	IDr, IDPr	18.1	3	2	2	9	3		
2035	FG301	40		sfrC	ISs+s·r, IDs+s·r, Fs+s·r	21.1			8	8	8		
2036	B52	20	M	sfrC	Sr, SEr	27.3	2	5			1		
2037	FG302	0	L	sfrC	Sr	(0.6)					5	2	3
2038	B53	(0)		sfrC	Sr, Dr	0.8					7	15	1
2039	FG303	0		sfrC	Sr, Ir	2.1				3	4	11	4
2040	B54	0		sfrC	Sr, Ir	0.3					2	10	3
2041	FG304	—		—	Sr, SPr	5.4				7	9		
2042	B55	30	M	sfrC	Sr, SPr, Dr	9.7				20	22	3	
2043	FG305	30		—	Dr, IDr	3.2				4	9	2	
2044	B56	40		sfrC	IDs+s·r, IDPs+s·r, DPs+s·r	14.8		2	11	21	11		
2045	FG306	60	H′	sfrC	IDs+s·r, DPs+s·r, ISs+s·r	23.1			3	11	10		
2046	P206	—		sfrC	IDPs+s·r	—				(4)			
	FG307	40	M	sfrC	ISs+s·r, IDs+s·r, IDPs+s·r	20.0		1	3	11	3		
2047	D464	—		—	Ds·r+r, Ds+r, IDs·r+r	—							
2048	D465	—		—	ISr, SEr, IDPr	—							
	FG308	30		—	ISr, SEr, IDPr	(8.1)			4	4	1		
2049	P207	—		sfrC	Dr	—				1	1		
	FG309	0	L	sfrC	Sr	tr.							1
2050	P208	—		sfrC	IDs+s·r	—					1		

- ( ): doubtful data
- —: no available data
- tr: <0.1kg/m²
- Size distribution: numbers of nodules in each fraction.
- buried nodules in piston cores: Depth from core top in cm in Position column.
- sed. type (sfr: siliceous fossils rich, s: siliceous, p: pelagic, zr: zeolite rich, C: clay).

(continued)

nodules

Total weight (g)	Position on/in sediment	Internal Structure	Nucleus	Polynucleation (%)	Associated material
2772		do.		0	shark teeth, pumice
2746	most buried, few partly exposed	do.		10	shark teeth, pumice, micronodules
2440		irregular nodule fragments, surrounding layers		10	
4145	partly exposed	compact nodules inside, surrounding layers (~1cm)		0	shark teeth, micronodules
68		concentric bands		0	
116	most buried, few partly exposed	do.	shark tooth	0	pumice, shark teeth, benthic foraminifera
239		do.		0	shark teeth, pumice
49		do.		0	do.
620		do.		40	
1479	completely buried	compact nodules inside, surrounding layers (~1cm)		40	benthic foraminifera
371		do.		20	pumice
2254	exposed (half buried)	compact and fractured nodules inside, surrounding layers		50	benthic foraminifera
2676		do.		40	
137	2 nodules (-562)			0	
2308		irregular nodule fragments, surrounding layers		50	
~50kg				—	pumice
~300kg				—	pumice, shark teeth
935				0	
108				0	pumice
1				0	
15				—	

Line I-a

ST 1987

B35	FG260
6.1 kg/m^2 $^{\Delta}$15% Ir, Dr, Sr, Ts+r	>3.4 kg/m^2 – % Sr, Dr, SPr, Ir

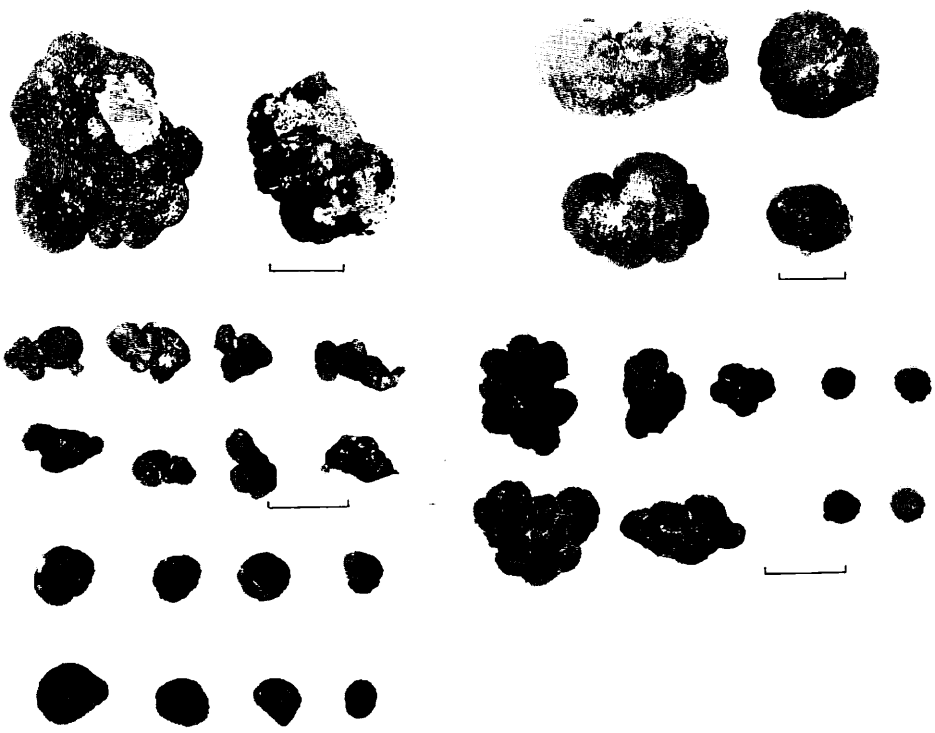

Appendix IX-2 (1)

Appendix IX-2(1-33) Sea-bed photography, top surface of box cores, and external morphology of manganese nodules collected on detailed survey lines (from north to south).

1) Data of each heading from the left to the right first: nodule abundance

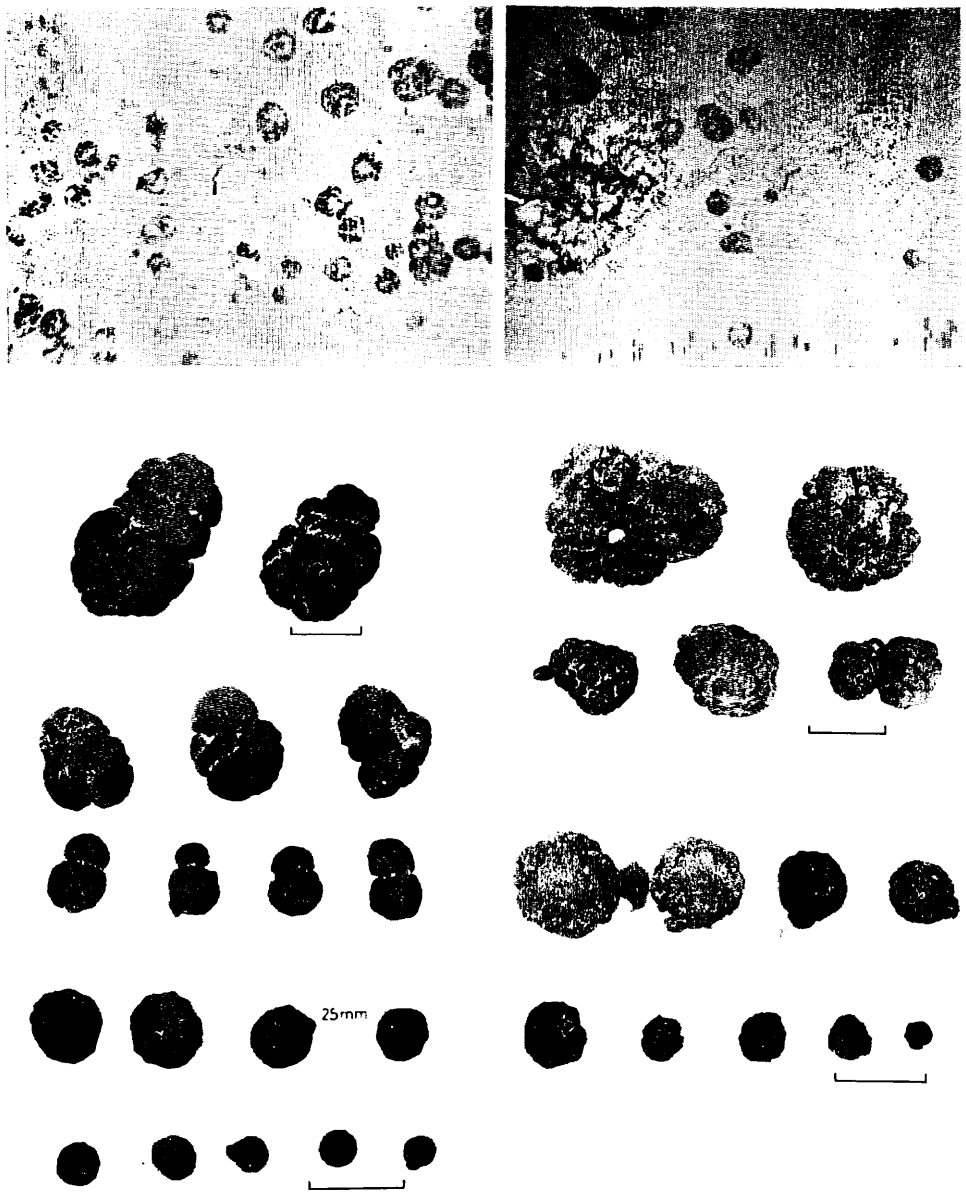

Appendix IX-2 (2)

(kg/m²), second: nodule coverage ratio (%), third: dominant morphological type.

2) Data with a small triangle is uncertain. —: no available data.

3) Upper photos by 16 mm one-shot camera, trigger weight ca. 10 cm in

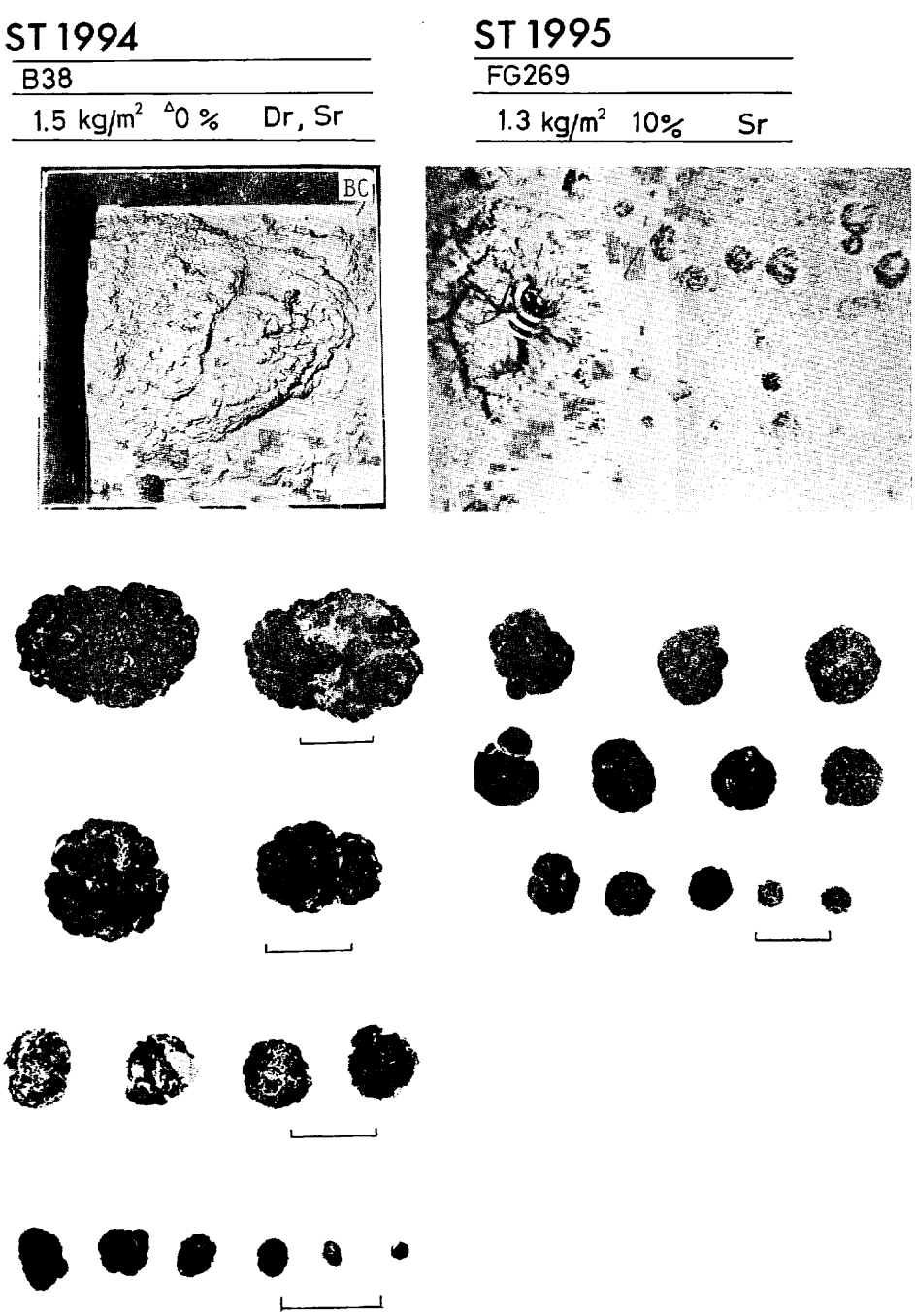

Appendix IX-2 (3)

diameter.

4) Photos with BC on the upper right corner: top surface of recovered box core, width of box core 40 cm.

5) Scale bar in photos of nodule samples: 25 mm.

ST1996

FG270

9.2kg/m^2 30% ISPs+s·r

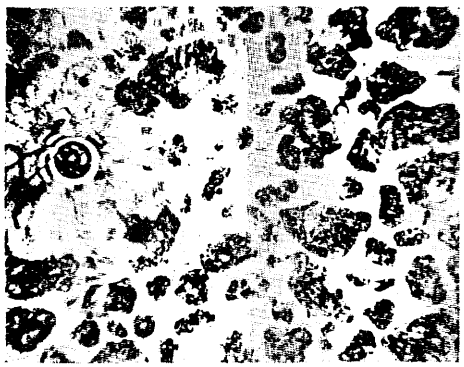

ST 1997

FG271

6.6 kg/m^2 20% Sr, SPr, Dr

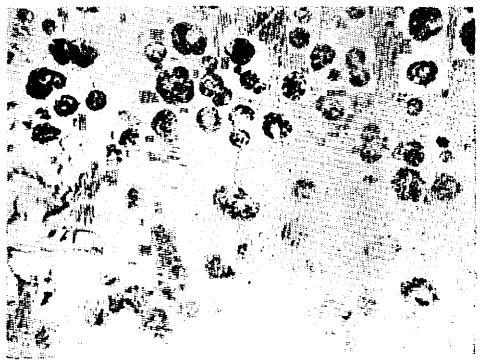

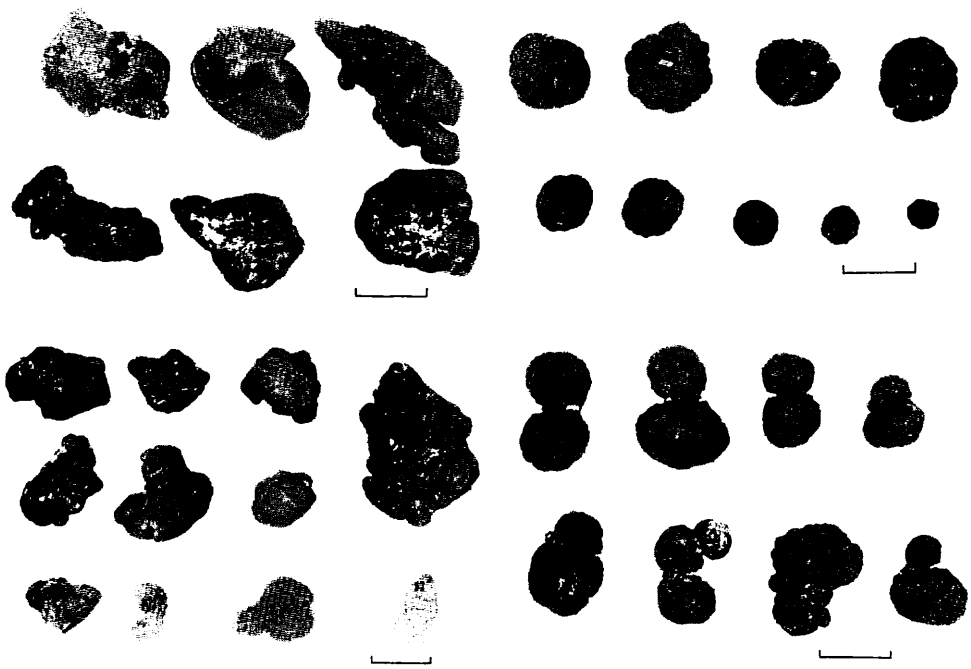

Appendix IX-2 (4)

ST 1998	ST 1999
B39	FG272
7.6 kg/m^2 △20% SPs-r+r, Ds-r+r, Dr	15.9 kg/m^2 30% IDPs+s-r, ISPs+sr

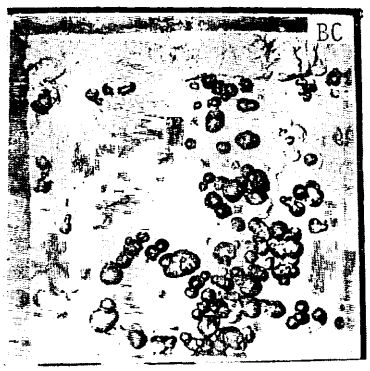

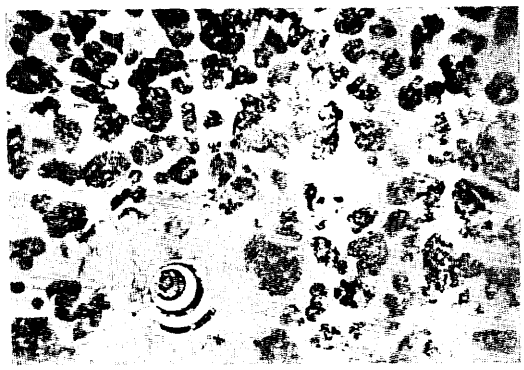

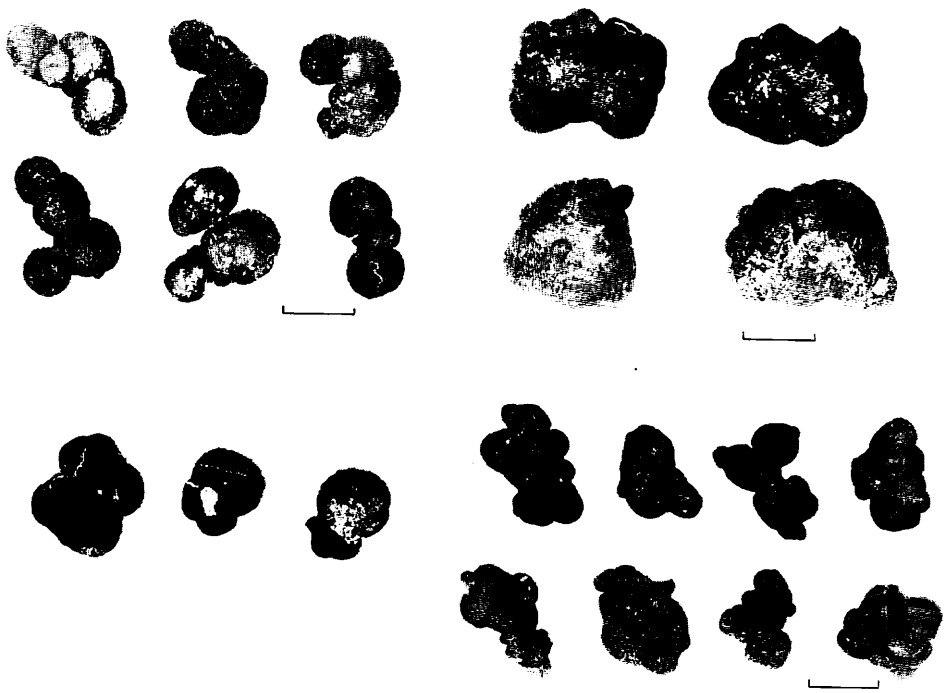

Appendix IX-2 (5)

ST 1986

FG259-1

28.0kg/m^2 60% IDPs+s·r, DPs

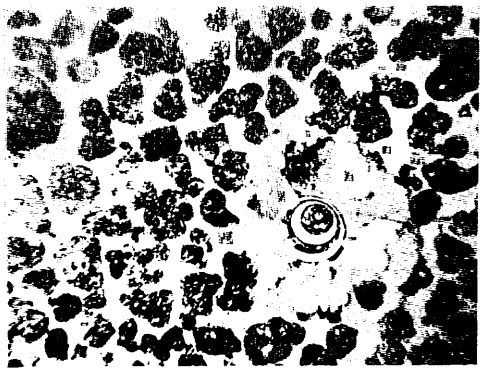

FG259-2

10.0kg/m^2 60% IDPs+s·r, DPs

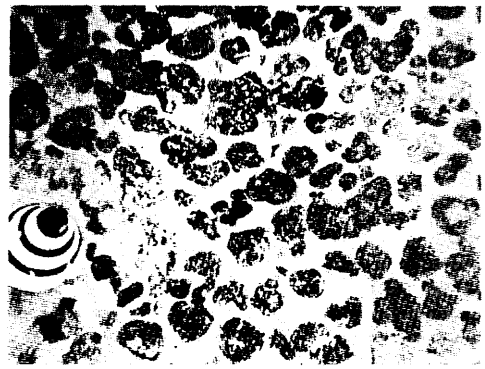

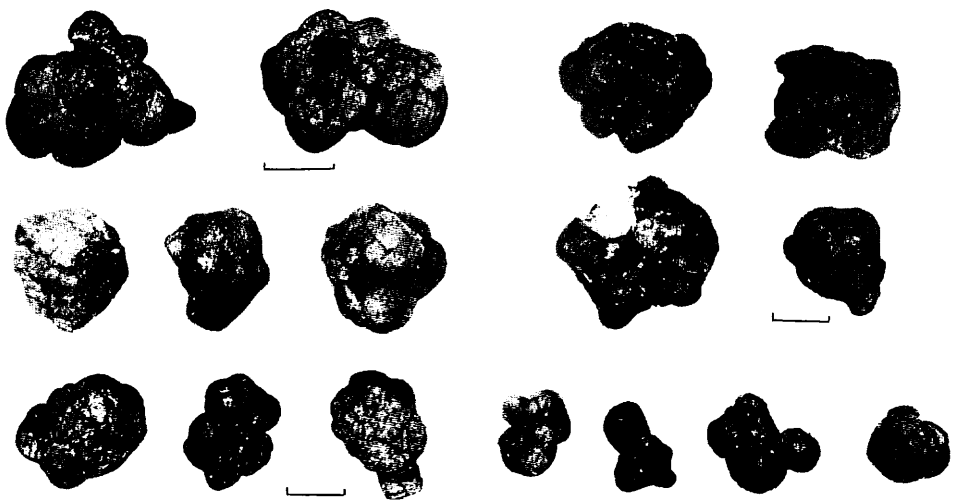

P196

— kg/m^2 — % IDs+s·r

Appendix IX-2 (6)

Line I-b

ST 1982

FG255-1

16.9kg/m² 70% IDs, Ds

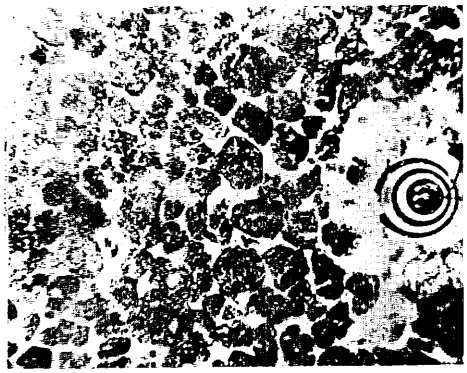

FG255-2

24.3kg/m² 70% IDs, Ds

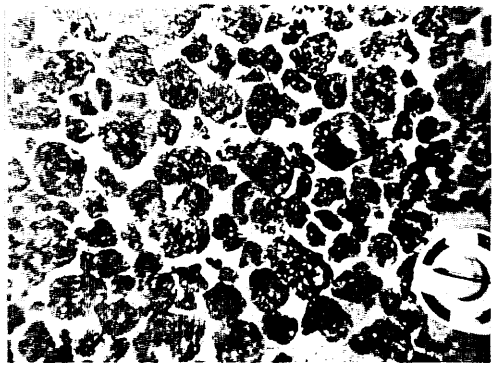

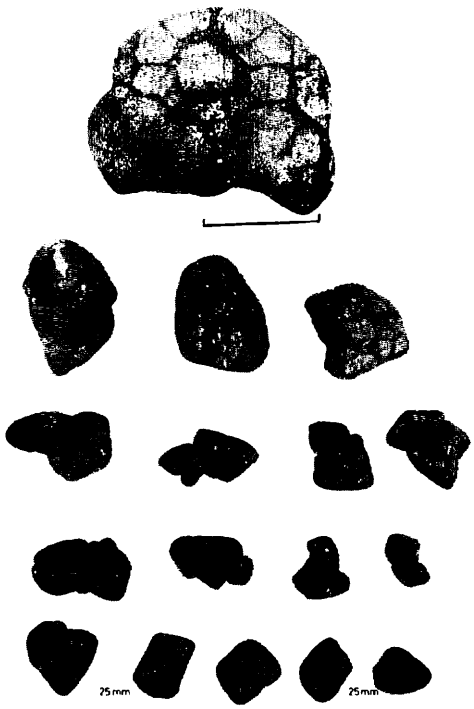

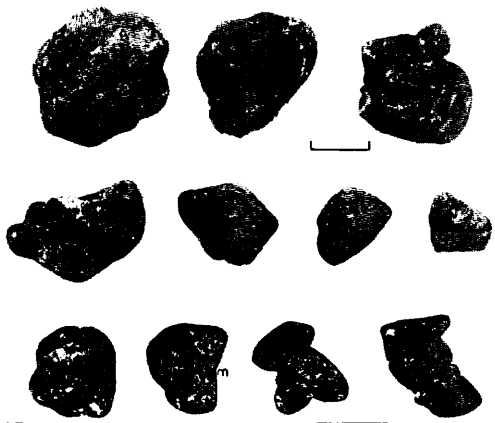

P193

— kg/m² — % IDs+sr

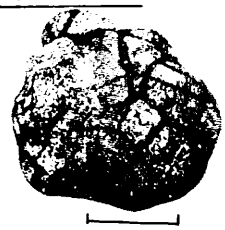

Appendix IX-2 (7)

ST 2000	ST 2001
FG273	FG274
13.3kg/m^2 70% ISs+sr, DPs+sr, Ds	24.5kg/m^2 60% IDPs+sr, DPs, ISs

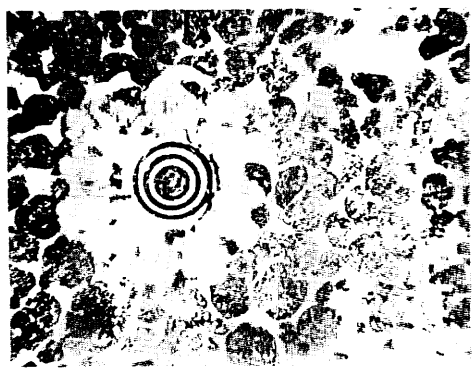

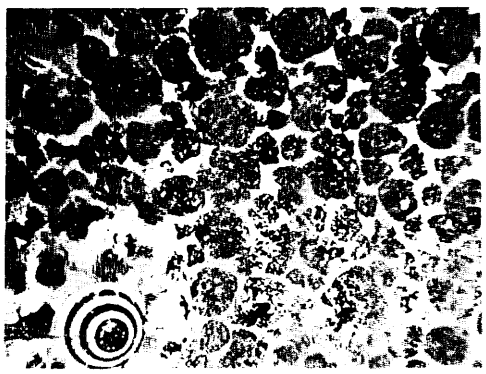

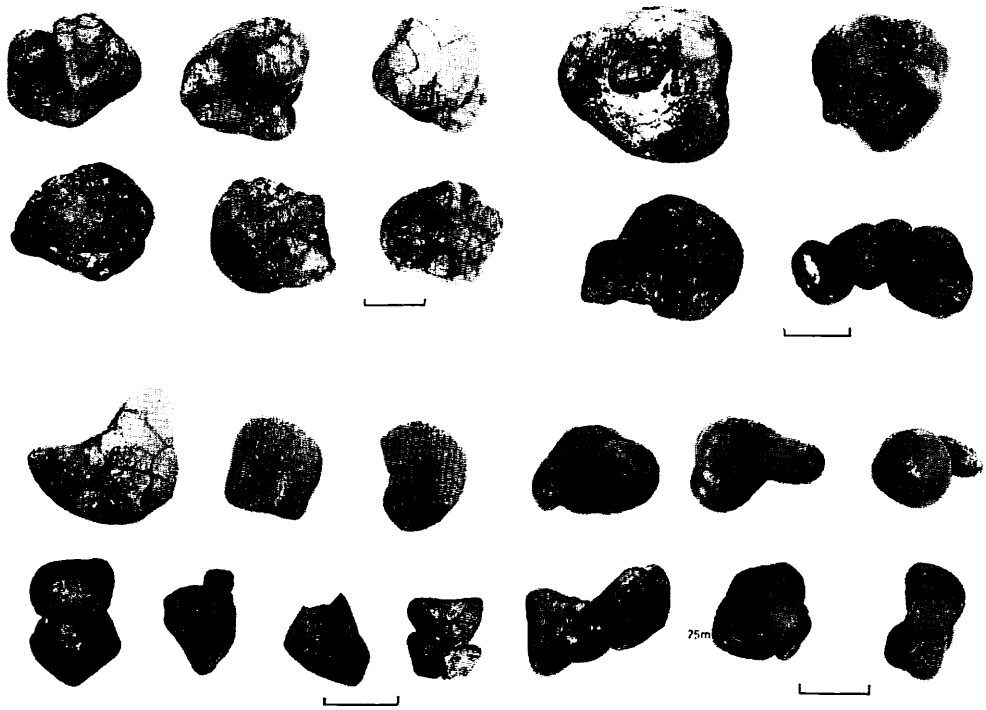

Appendix IX-2 (8)

ST 2002	ST 2003
FG275	B40
26.2kg/m^2 60% IDs+s·r, DPs+s·r, ISs	25.1 kg/m^2 $^{\Delta}$50% ISPs+s·r, IDPs+s·r

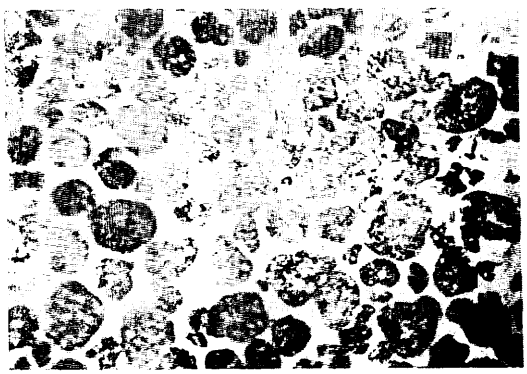

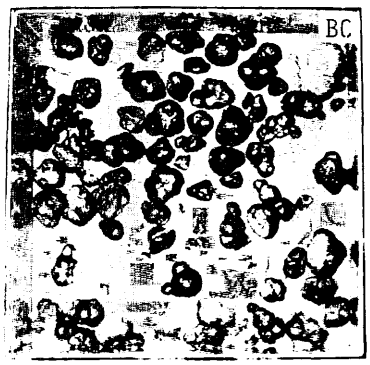

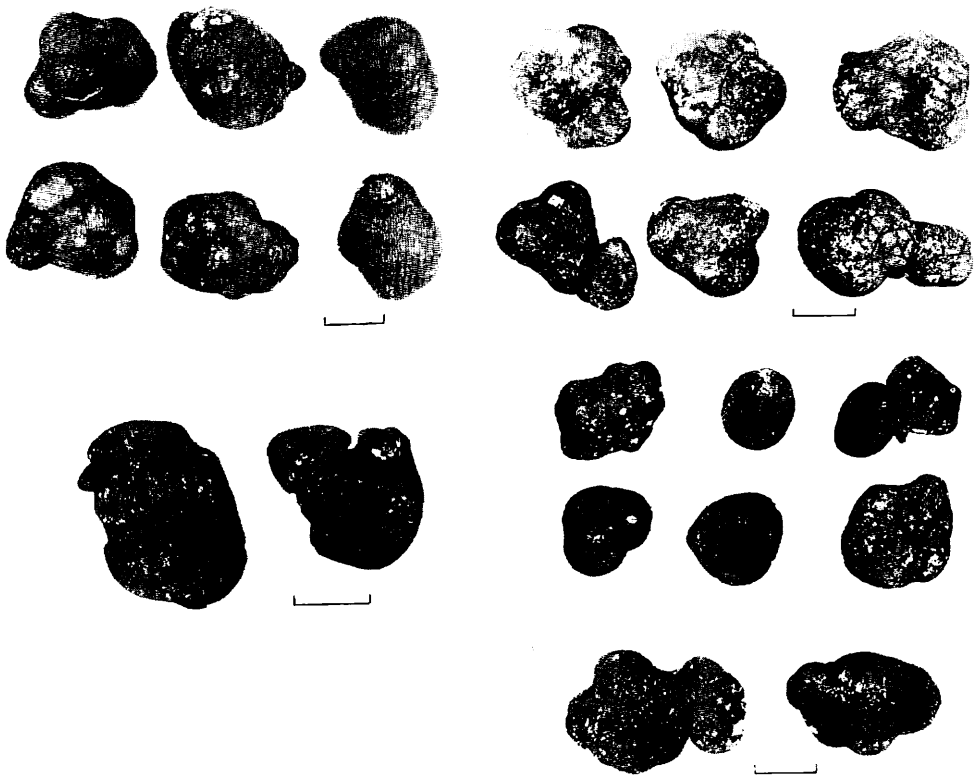

Appendix IX-2 (9)

ST 2004

FG276

21.4 kg/m^2 50% SPs+s·r, DPs+s·r

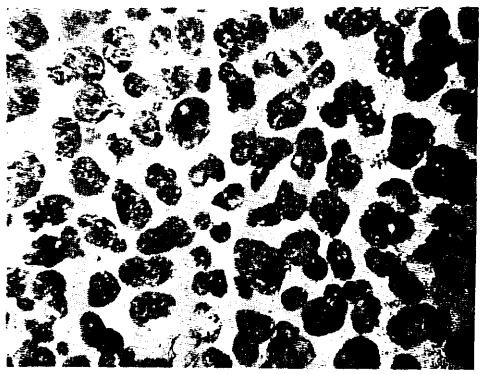

ST 2005

FG277

8.0 kg/m^2 40% SPs·r+r, Sr, Ds·r+r

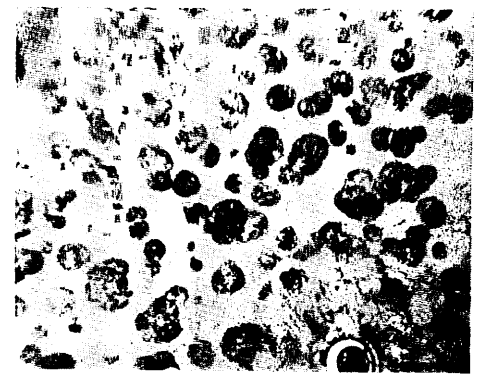

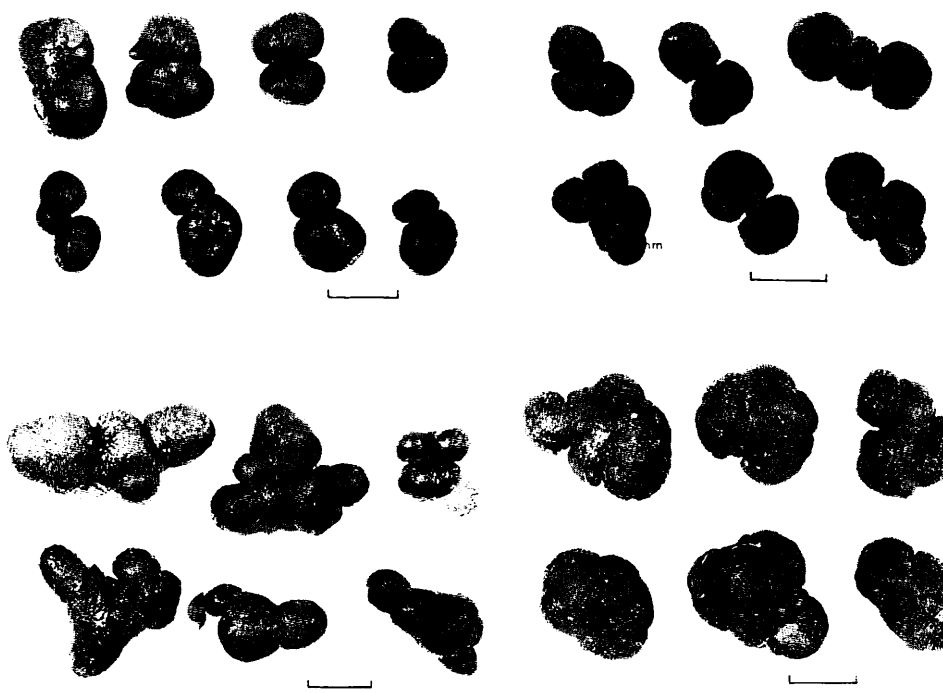

Appendix IX-2 (10)

ST 2006

P199

— kg/m² — % Sr

ST 2007

FG 278

4.4 kg/m² 10% Sr, Dr

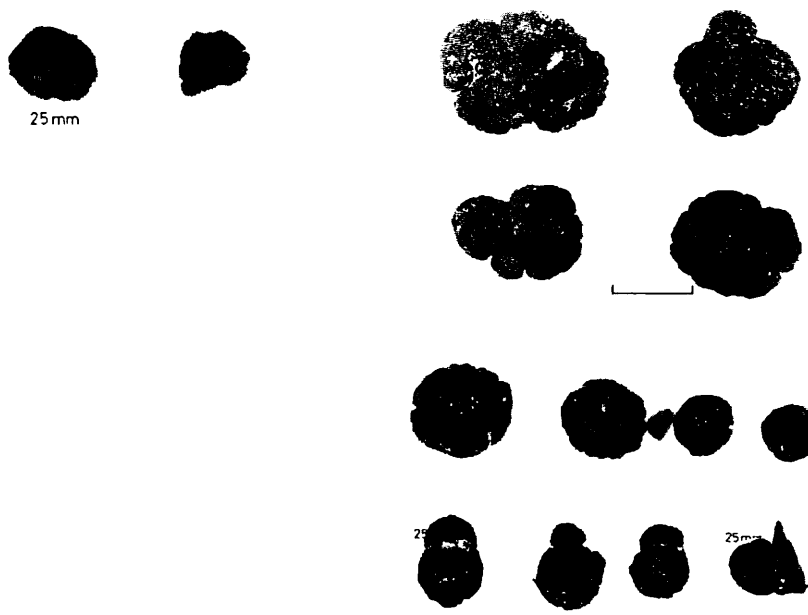

Appendix IX-2 (11)

ST 1981

B33

5.8 kg/m² Δ5% Sr, Dr

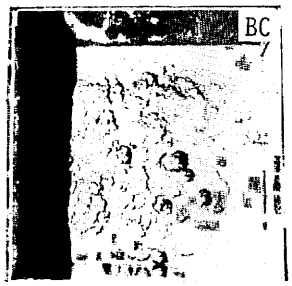

FG254

3.8 kg/m² 10% Sr, Dr

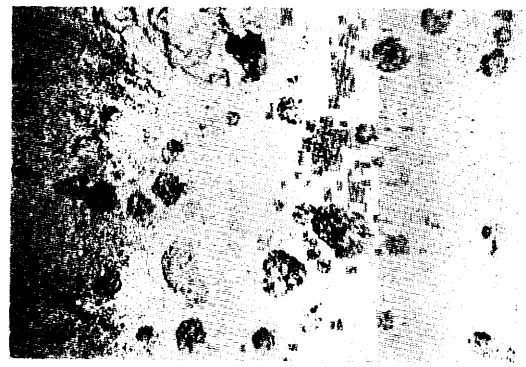

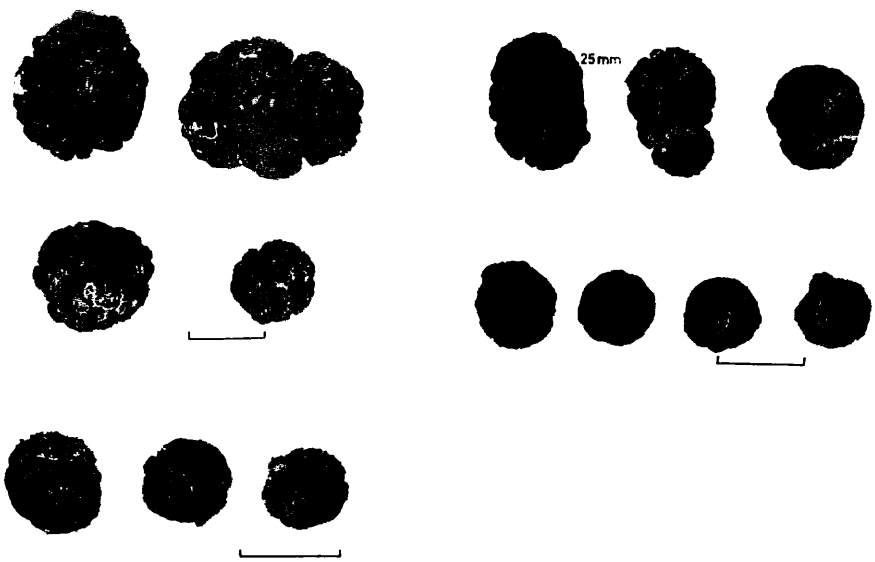

Appendix IX-2 (12)

ST 2008

FG279

>0.9 kg/m² 20% Dr, Sr

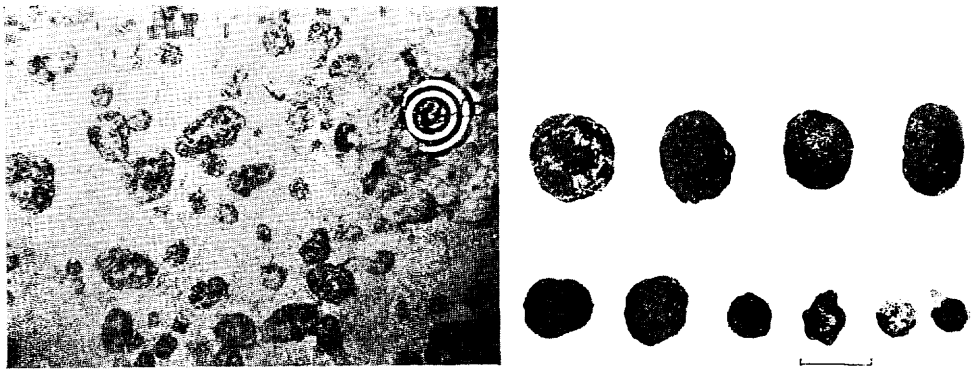

ST 2009

FG280

>0.9 kg/m² 15% Sr

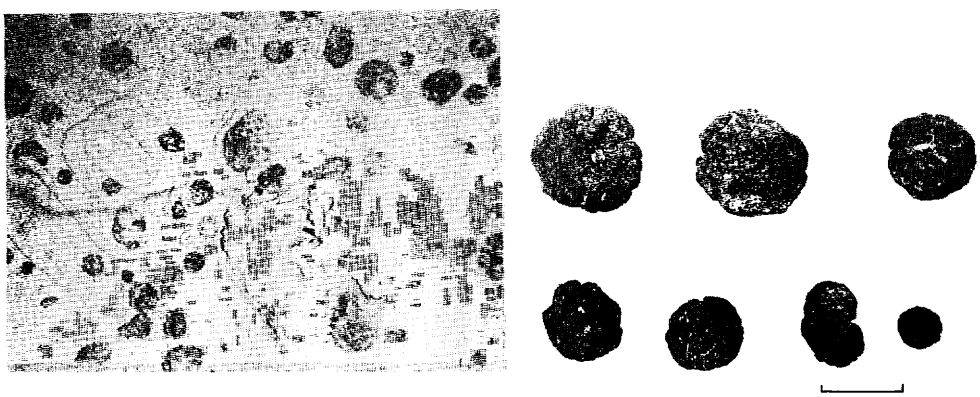

Appendix IX-2 (13)

ST 2010

FG 281

64 kg/m^2 20% Sr, Dr, SPr

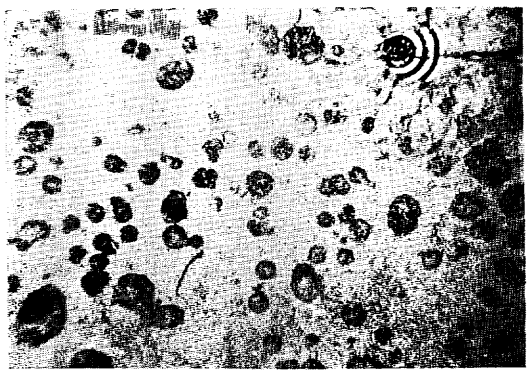

ST 2011

P200

— kg/m^2 — % —

ST 2011A

H44

— kg/m^2 — % Sr

Appendix IX-2 (14)

ST 2012

FG 282

0.2 kg/m² 10% Sr

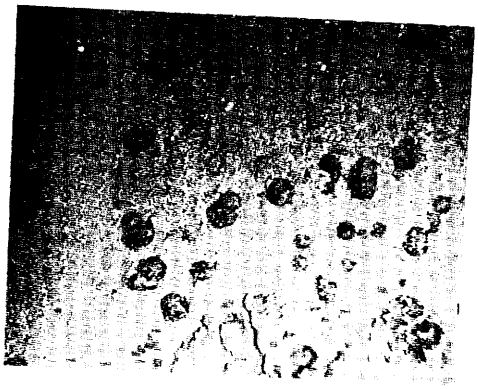

ST 2013

FG 283

>3.5 kg/m² 10% Sr, Dr, SPr

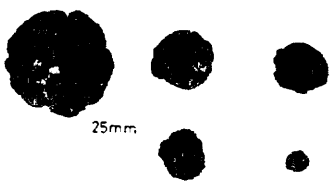

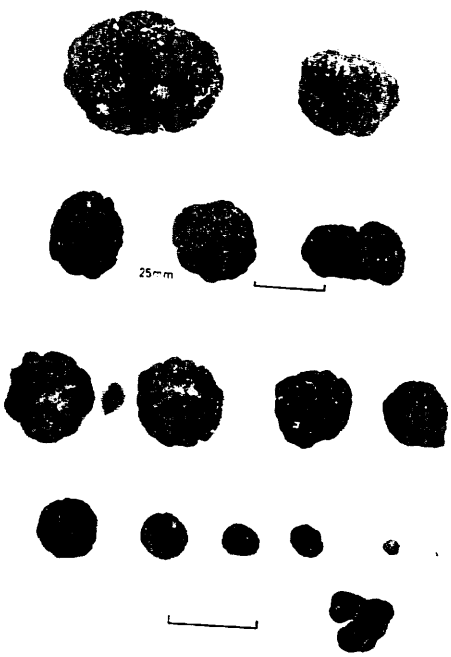

Appendix IX-2 (15)

ST 2014	ST 2015
B41	FG284
11.3kg/m^2 △30% Ds·r+r, Sr, IDPs·r+r	11.5kg/m^2 25% IDPs,ISs,IDPs+s·r

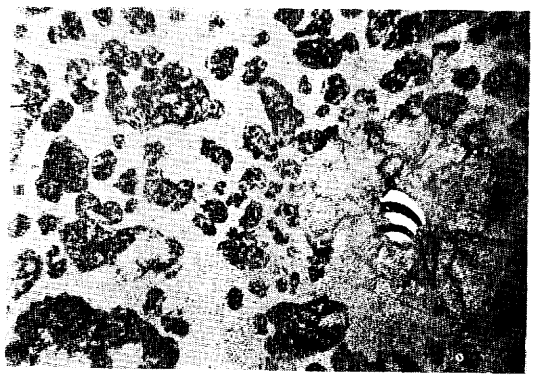

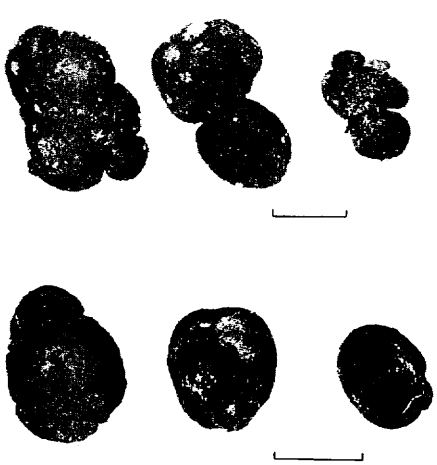

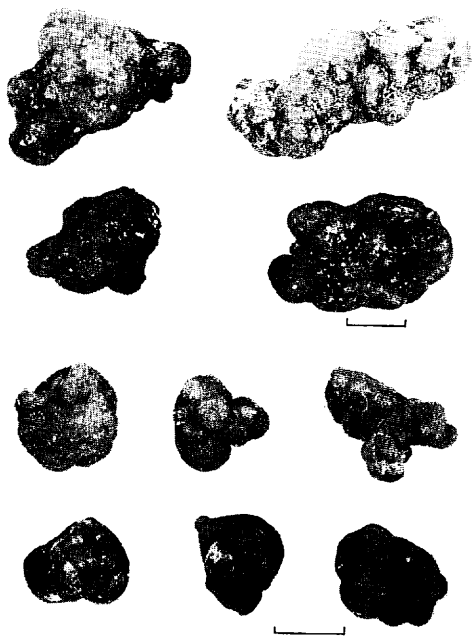

Appendix IX-2 (16)

ST 1980

FG 253

18.7 kg/m^2 30% IDPs+s·r, Ts+r, Ds+s·r

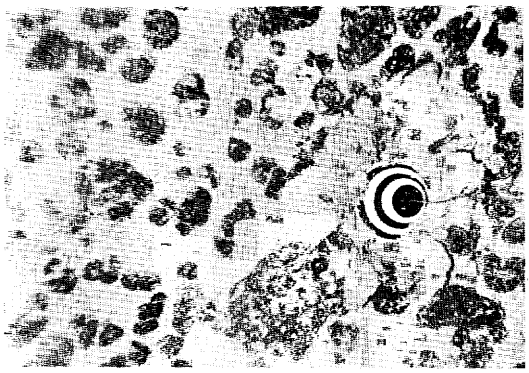

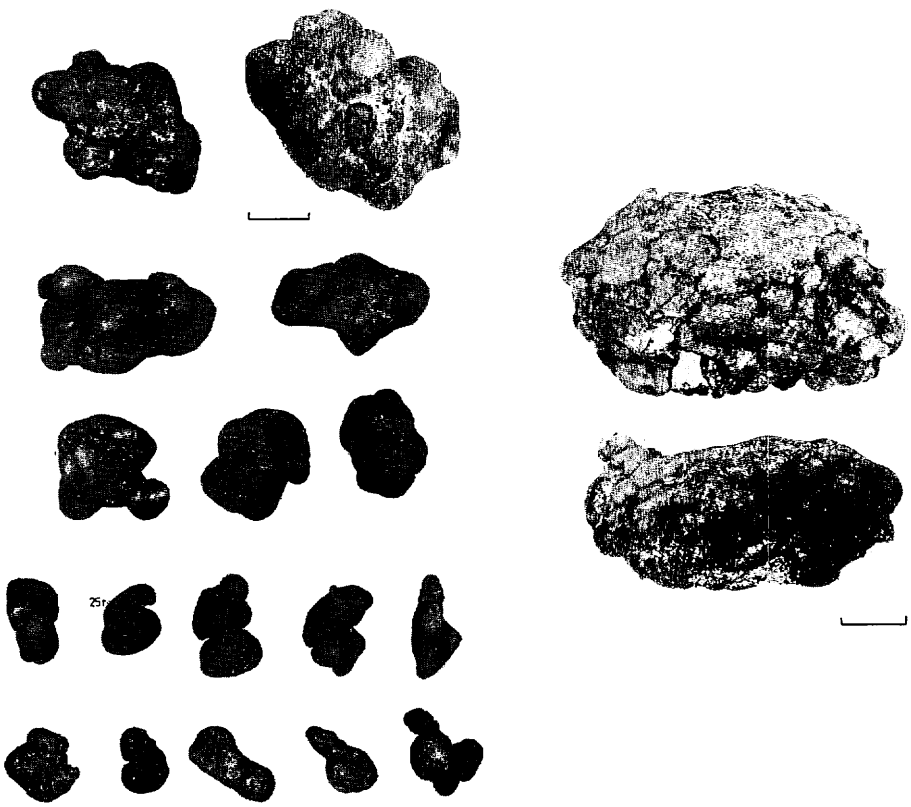

Appendix IX-2 (17)

Line II-a

ST 2021

FG290-1

>0.7 kg/m^2 0% Sr, Dr

FG290-2

2.8 kg/m^2 0% Dr, Sr

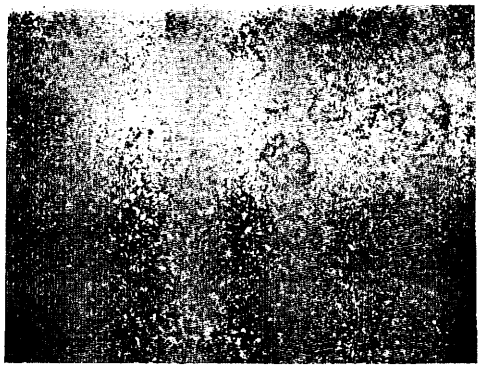

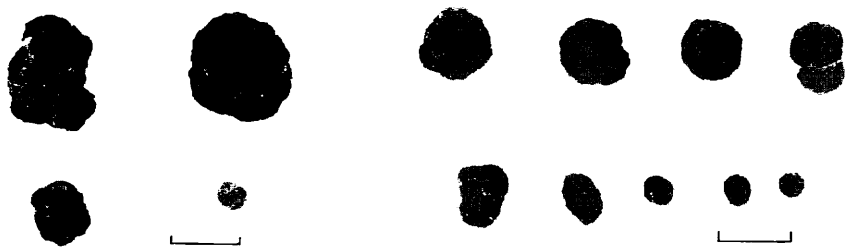

P202

— kg/m^2 — % Sr

Appendix IX-2 (18)

ST 2041

FG304

5.4 kg/m^2 — % Sr, SPr

ST 2042

B55

9.7kg/m^2 30% Sr, SPr, Dr

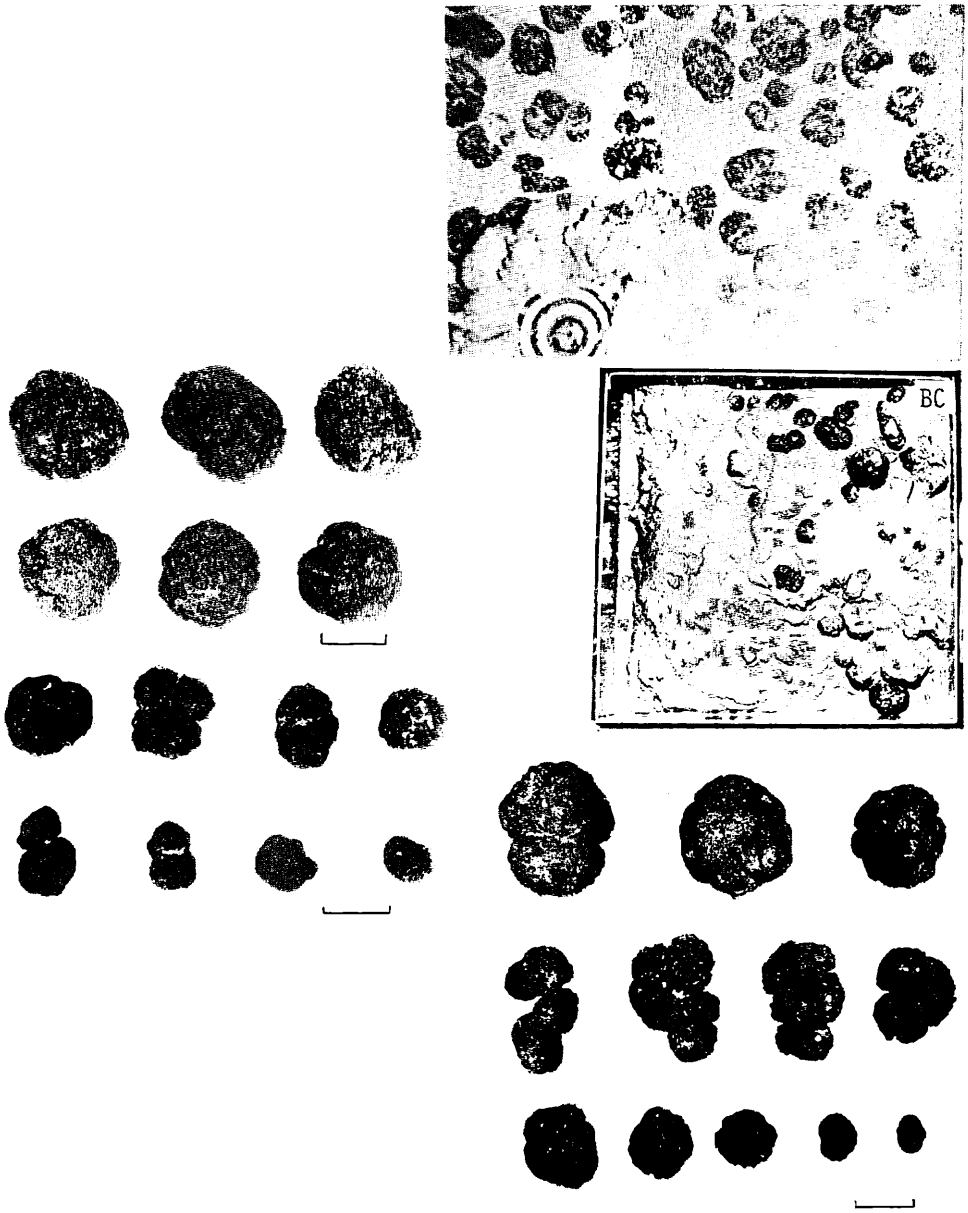

Appendix IX-2 (19)

ST 2043

FG305

3.2 kg/m^2 30% Dr, IDr

ST 2044

B56

14.8 kg/m^2 40% IDs+s·r, IDPs+s·r, DPs+s·r

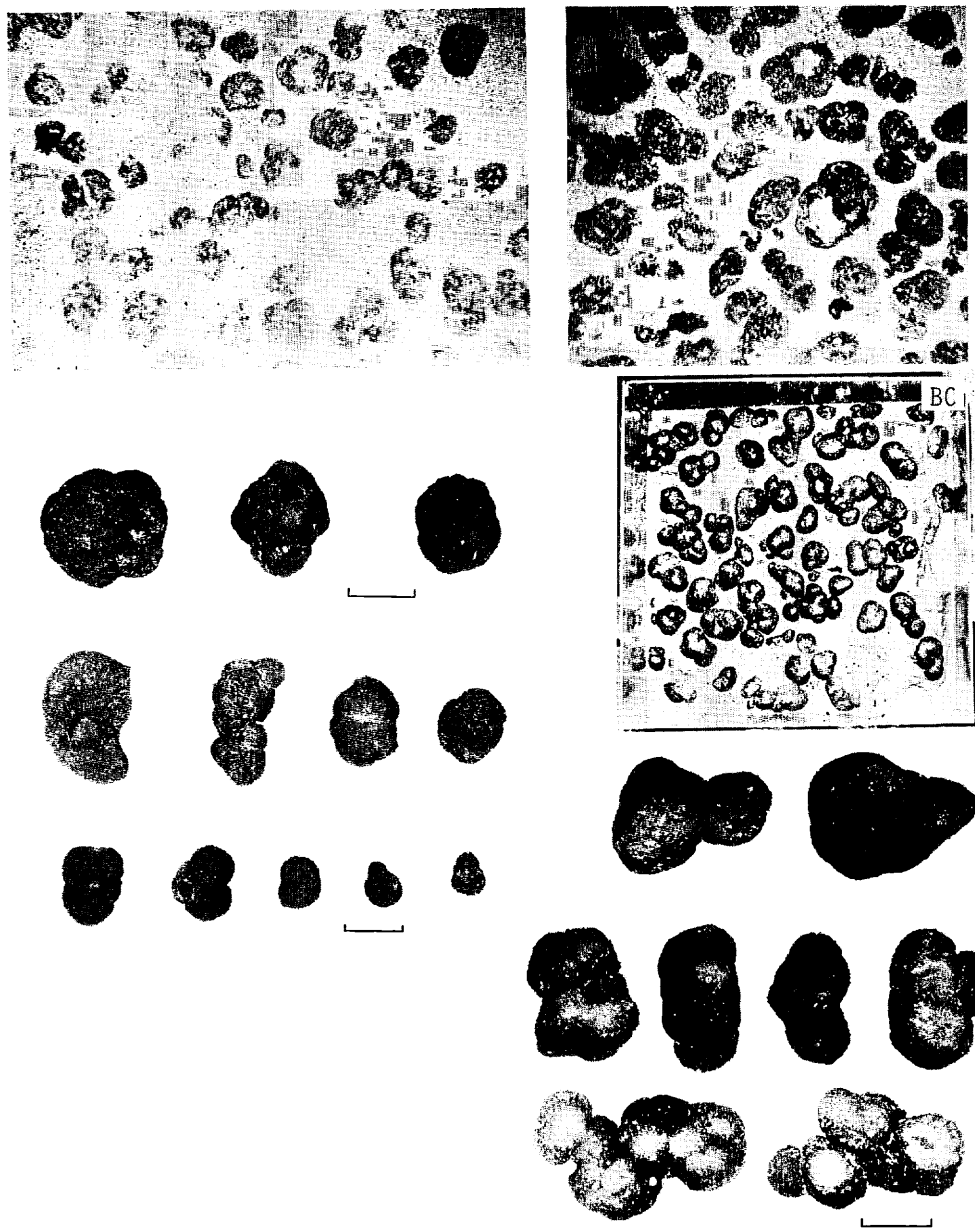

Appendix IX-2 (20)

ST 2046

FG307

20.0kg/m² 40% ISs+s·r, IDs+s·r

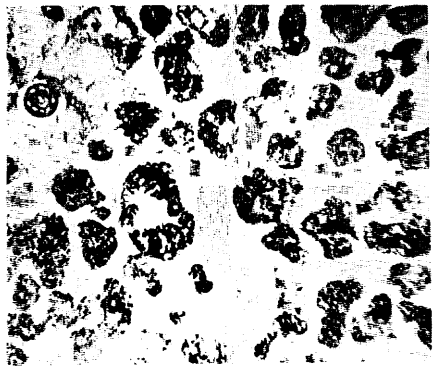

ST 2045

FG306

23.1 kg/m² 60% IDs+s·r, DPs+s·r, ISs+s·r

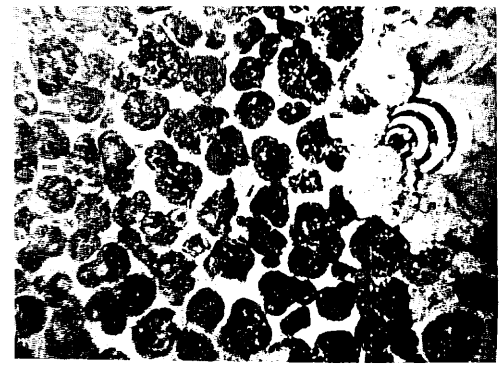

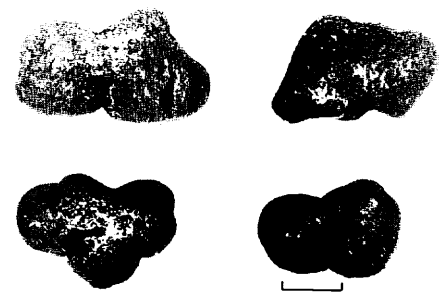

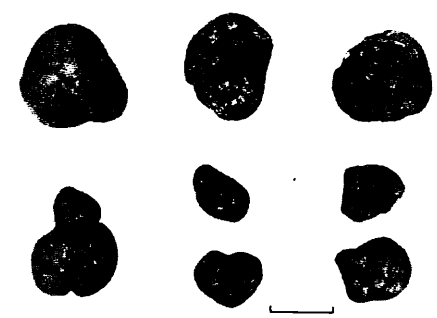

P206

— kg/m² — % IDPs+s·r

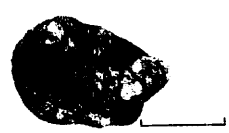

Appendix IX-2 (21)

ST 2022

B45	FG 291
24.4 kg/m² 50% IDs+s·r, ISs+s·r, IDs	20.5 kg/m² 50% IDPs+sr, ISs+s·r, Fs

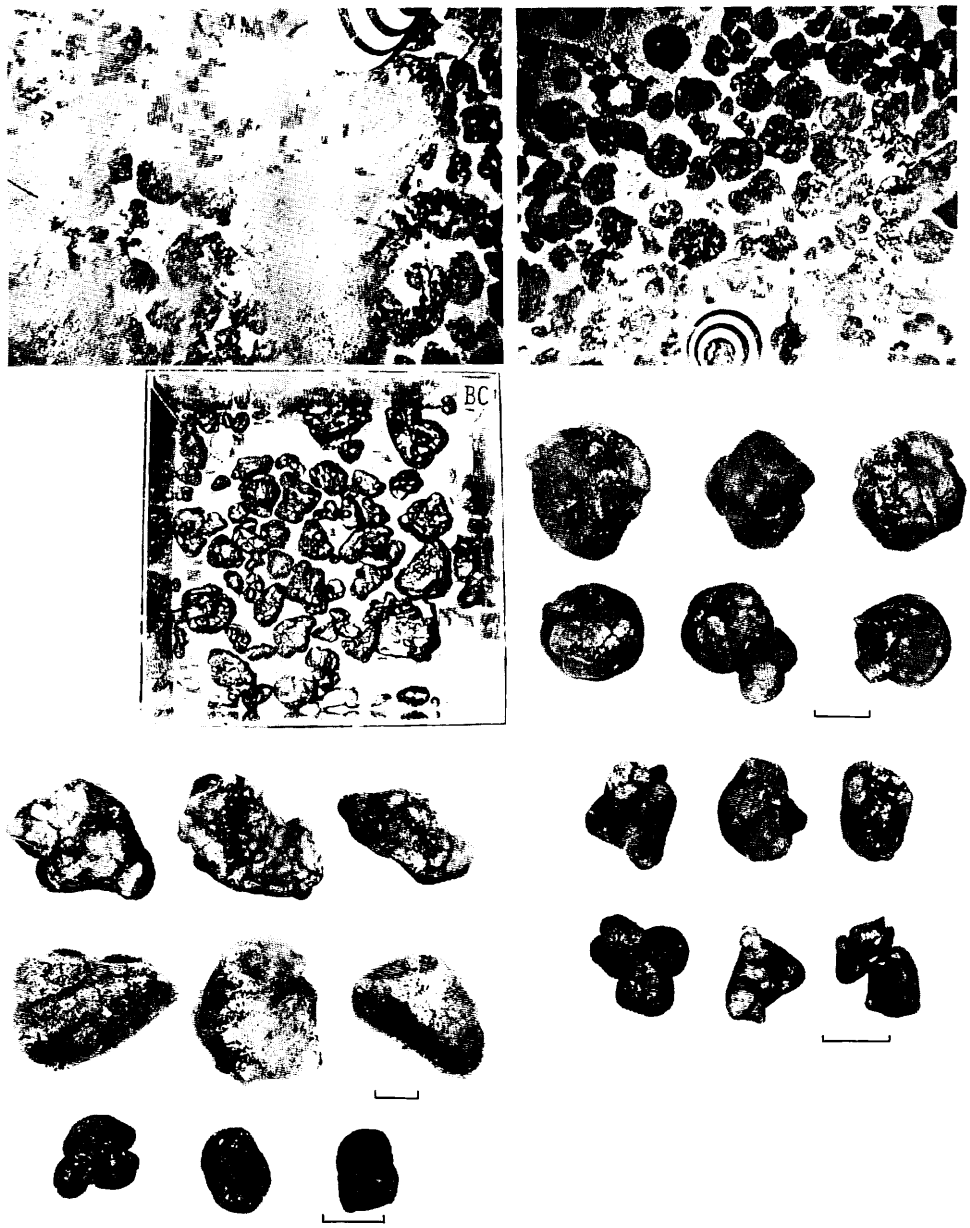

Appendix IX-2 (22)

Line II-b

ST 2026

FG 295-1

11.3kg/m² 25% IDPr, Dr, ISPr, Sr

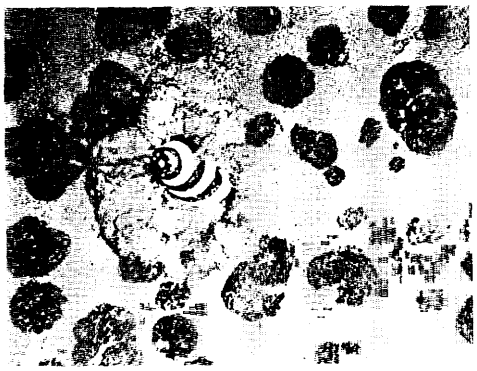

FG 295-2

13.9kg/m² 20% ISPr, IDPr, Dr

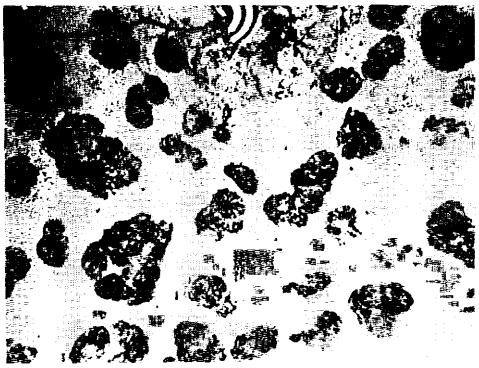

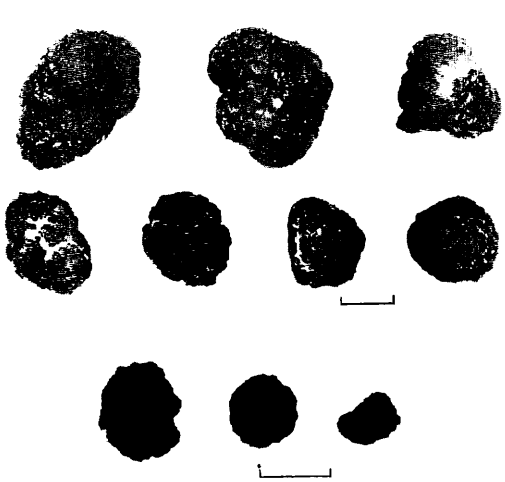

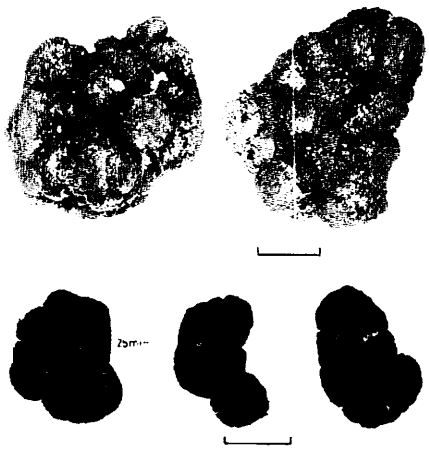

P204

— kg/m² — % SPr

Appendix IX-2 (23)

ST 2048

FG308

>8.1 kg/m^2 30% ISr, SEr, IDPr

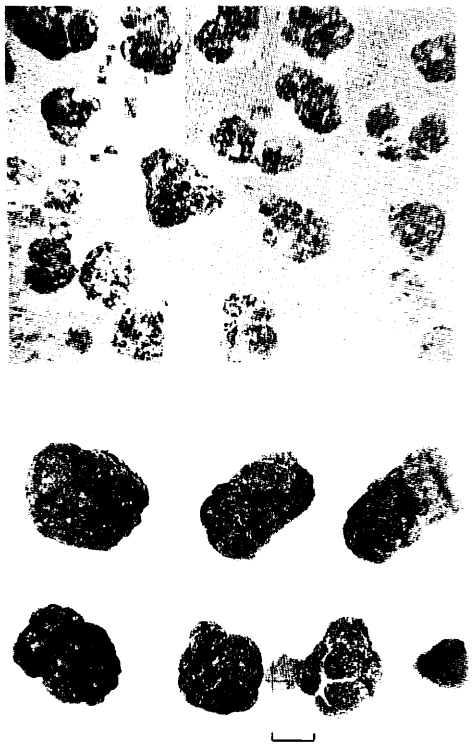

ST 2034

B51

18.1 kg/m^2 20% IDr, IDPr

Appendix IX-2 (24)

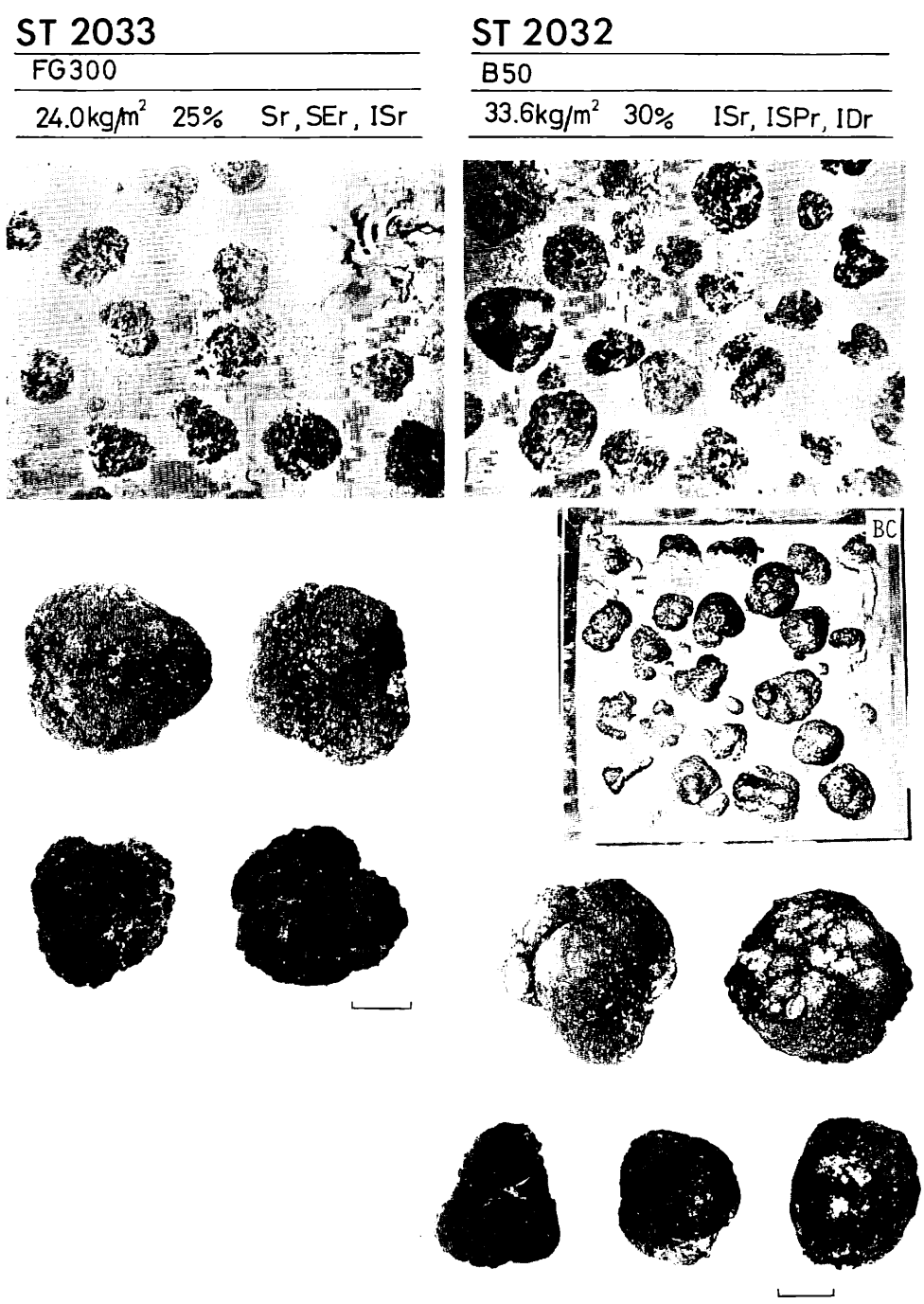

Appendix IX-2 (25)

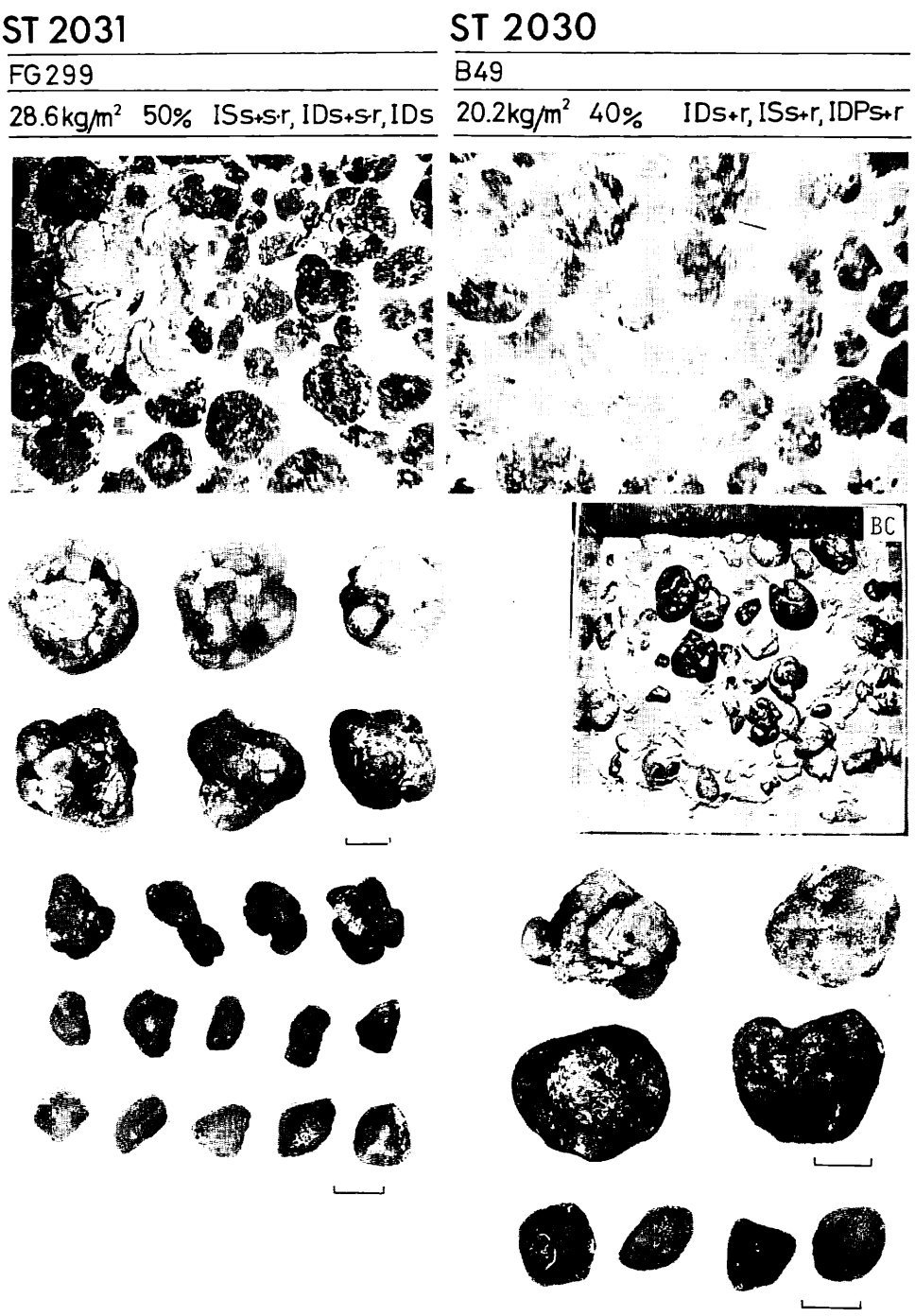

Appendix IX-2 (26)

ST 2029

FG 298

19.9 kg/m² 50% IDs+s·r, ISs+s·r, IDPs+s·r

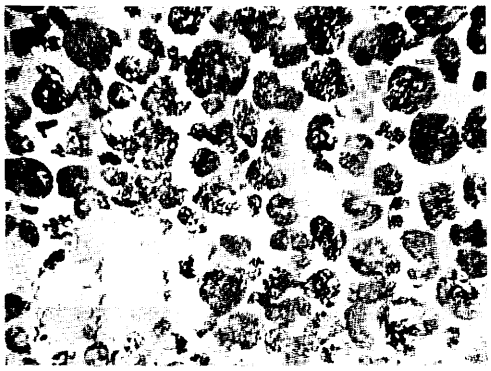

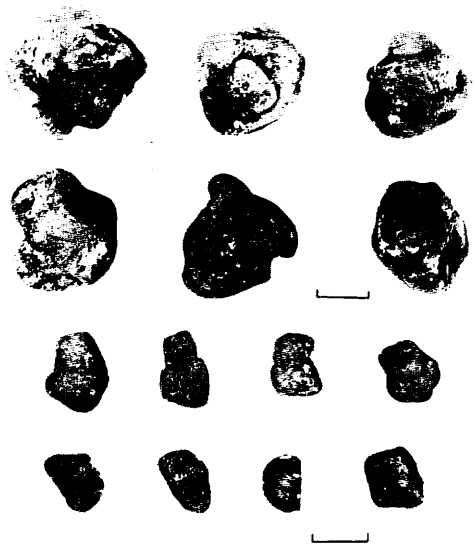

ST 2027

FG 296

1.7 kg/m² △30% Fs

Appendix IX-2 (27)

(ST 2027)

B48

10.6 kg/m^2 60% IDs, ISs, IDPs, IDs+sr

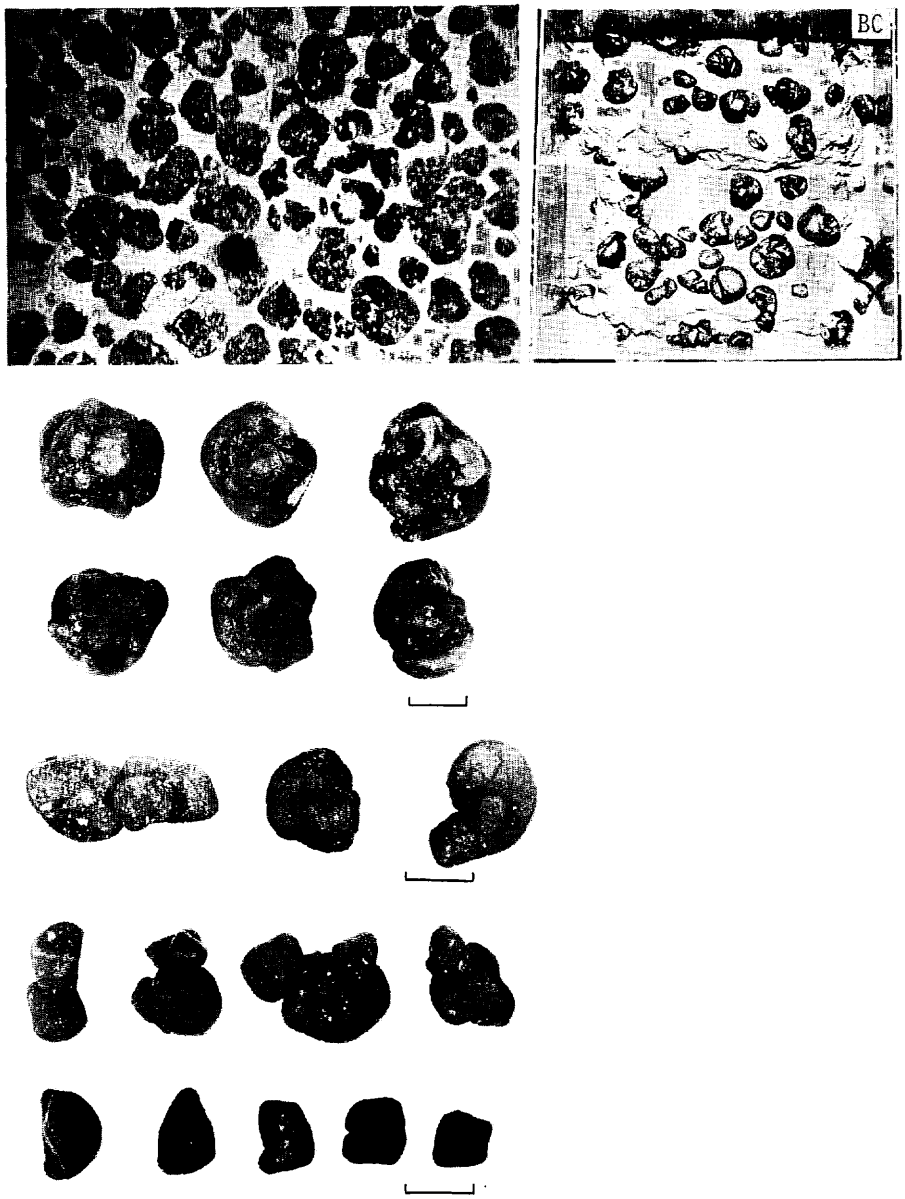

Appendix IX-2 (28)

Line II-c

ST 2018

FG 287-1		
1.3 kg/m^2	— %	Dr, Ir, Sr

FG 287-2		
1.0 kg/m^2	0%	ISr, Ir, Sr

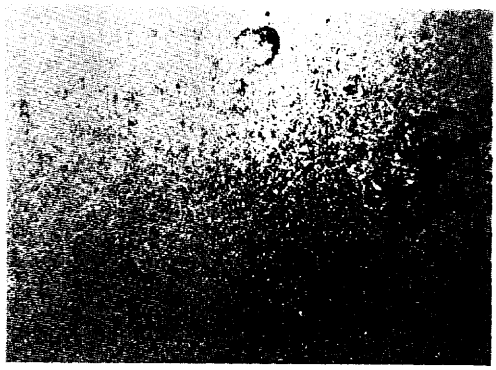

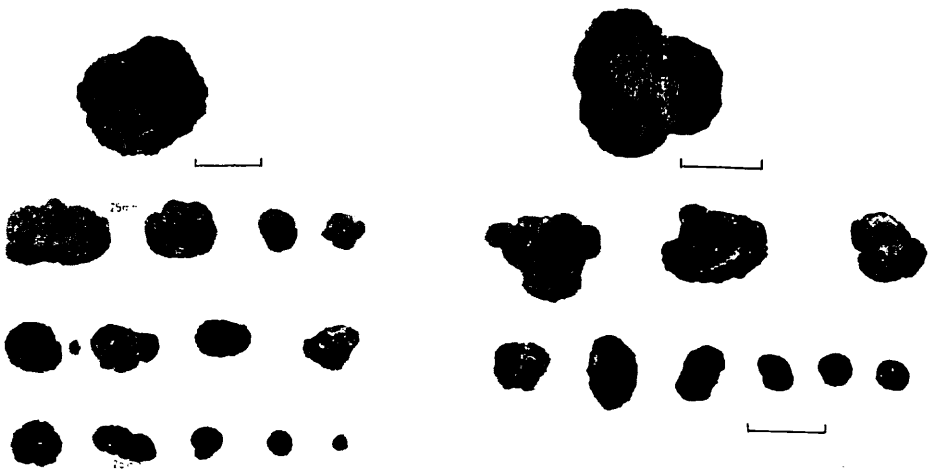

P 201		
— kg/m^2	— %	—

Appendix IX-2 (29)

ST 2040

B54

0.3 kg/m^2 0% Sr, Ir

ST2039

FG303

2.1 kg/m^2 0% Sr, Ir

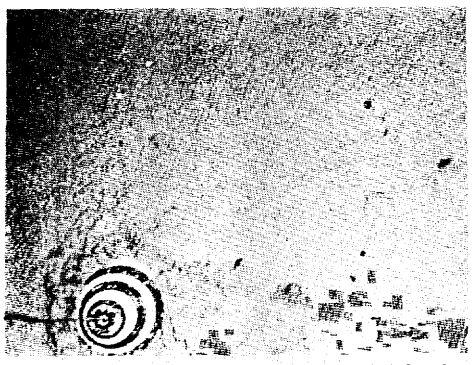

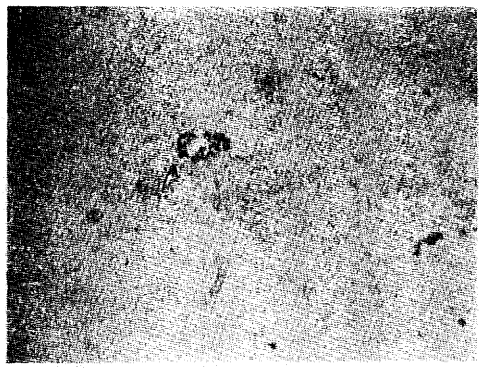

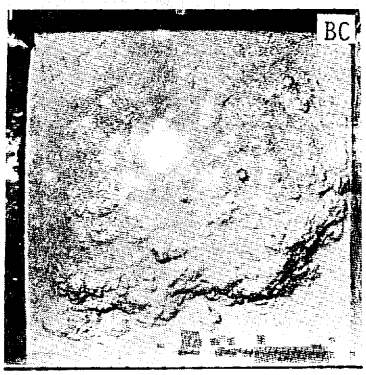

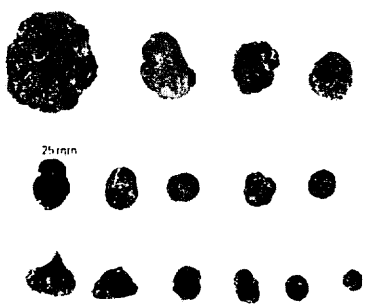

Appendix IX-2 (30)

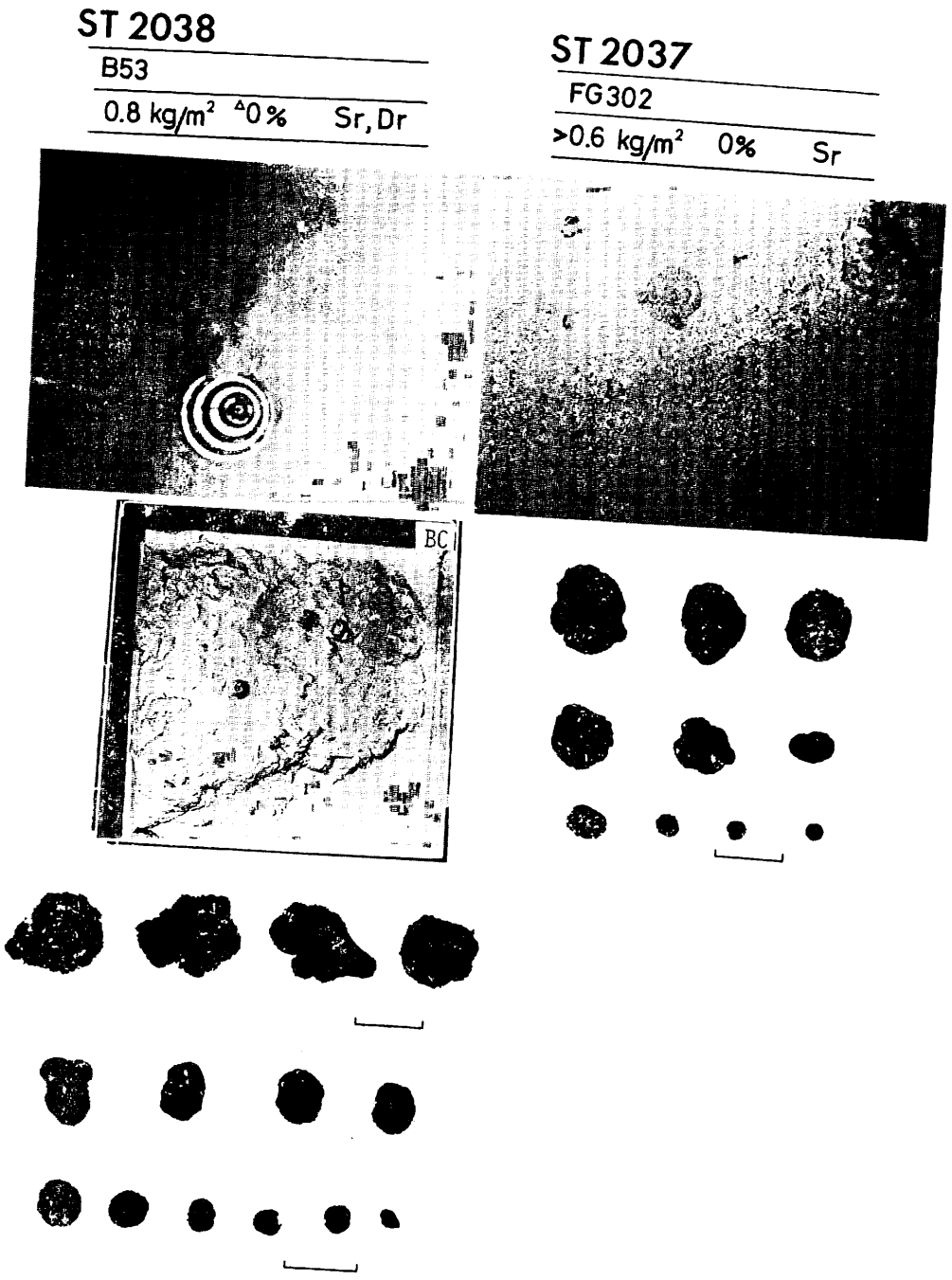

Appendix IX-2 (31)

ST 2036	ST 2035
B52	FG 301
27.3 kg/m² 20% Sr, SEr	21.1 kg/m² 40% ISs•s•r, IDs•s•r, Fs•s•r

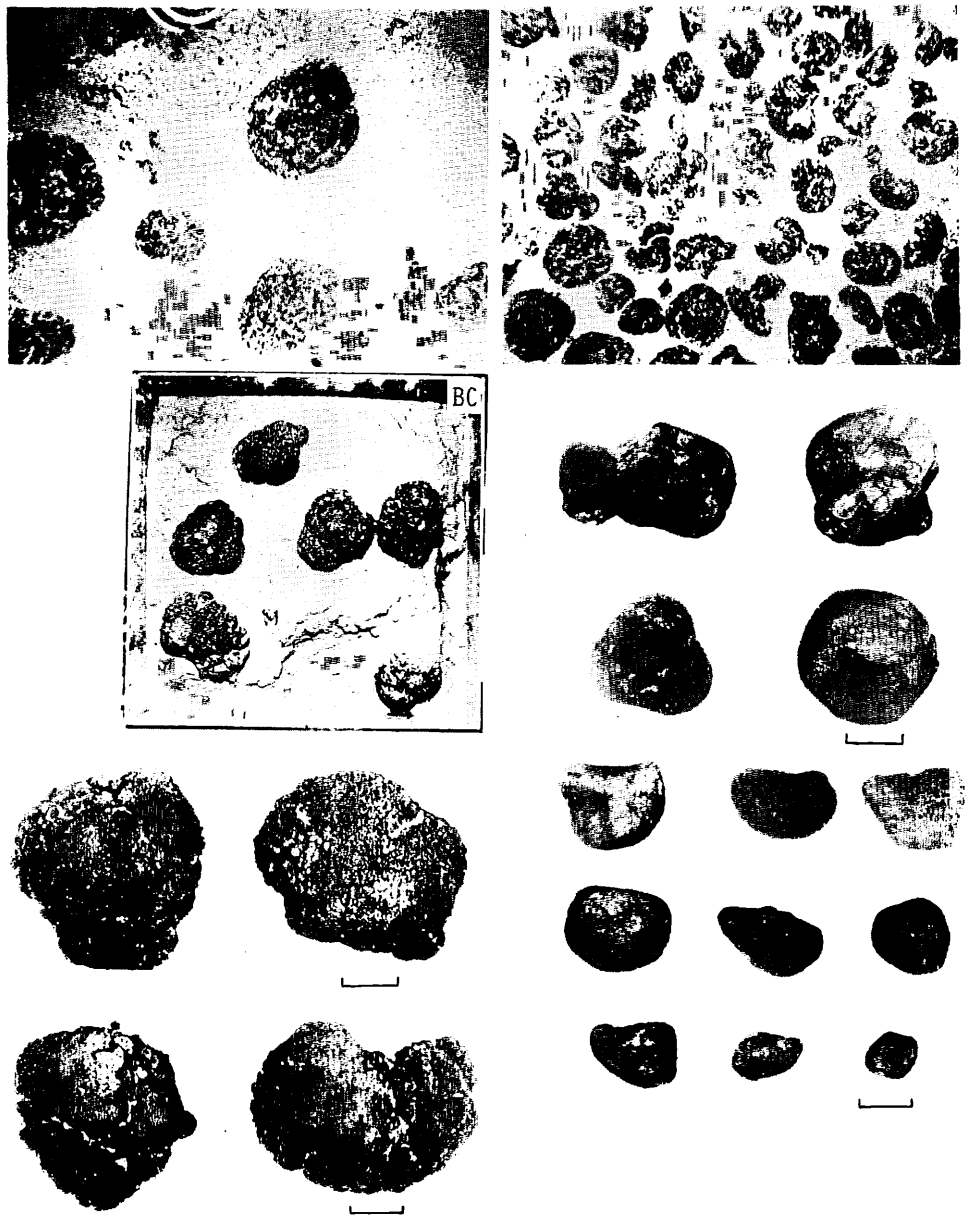

Appendix IX-2 (32)

ST 2017

FG 286

26.5kg/m² 50% ISs+s·r, IDs+s·r

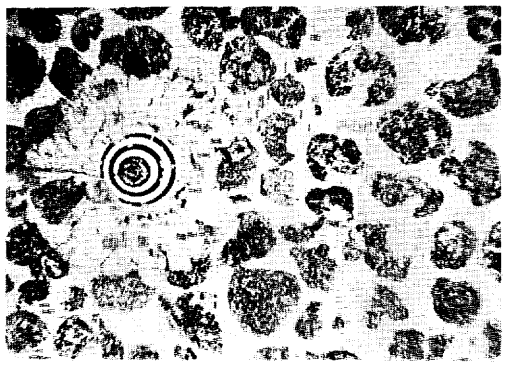

B42

23.6kg/m² ^50% ISs+s·r, DPs+s·r, Ds

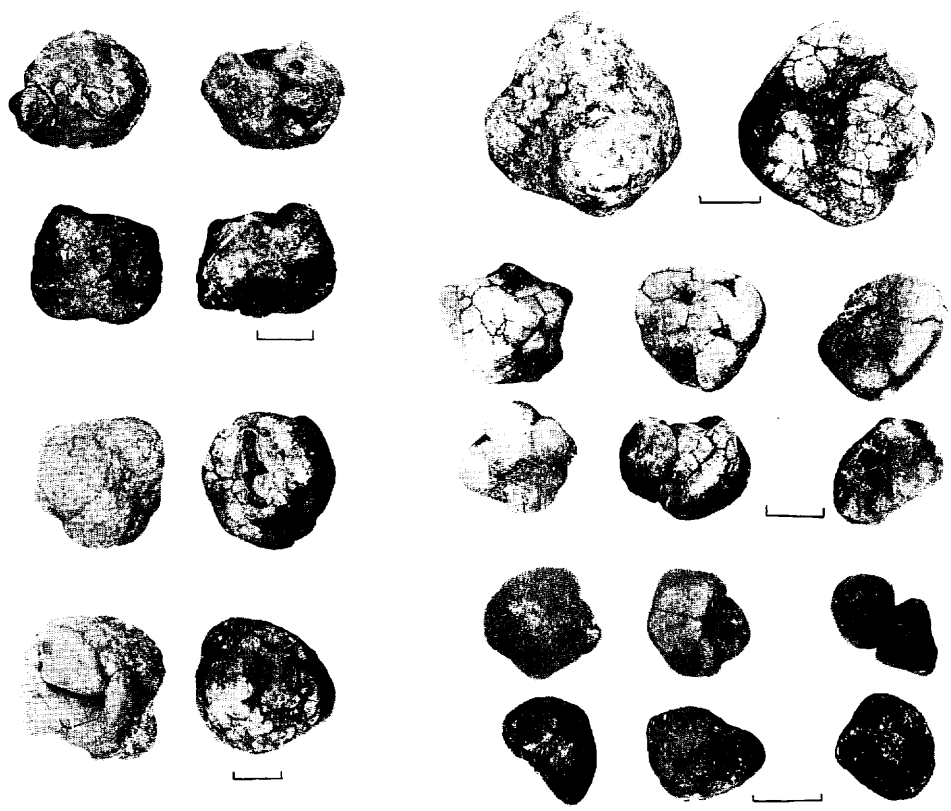

Appendix IX-2 (33)

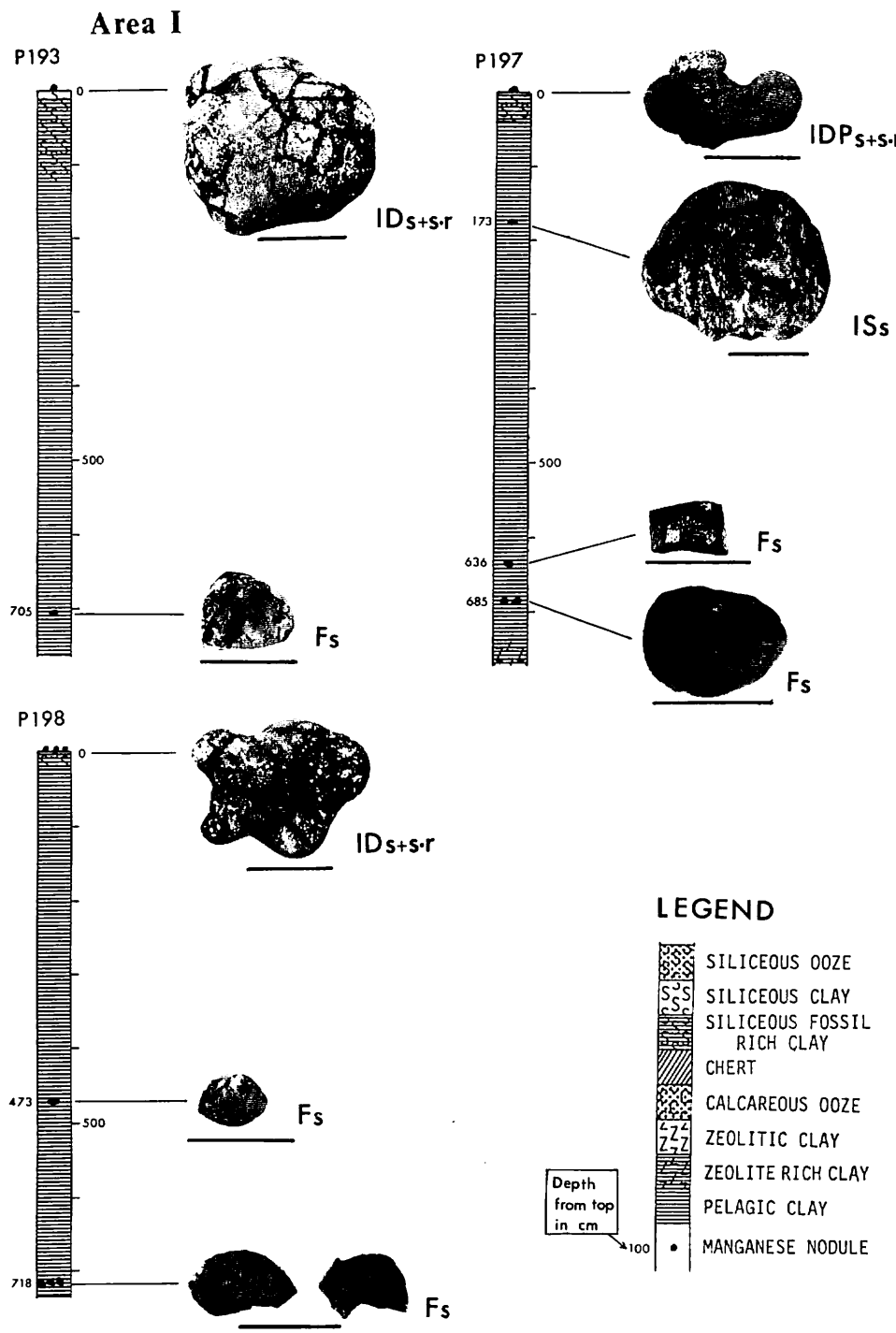

Appendix IX-3 (1)

Appendix IX-3(1, 2) Manganese nodules buried deep in sediment columns of piston cores. Symbols with nodules are morphological type. Scale bar: 1 cm.

Area II

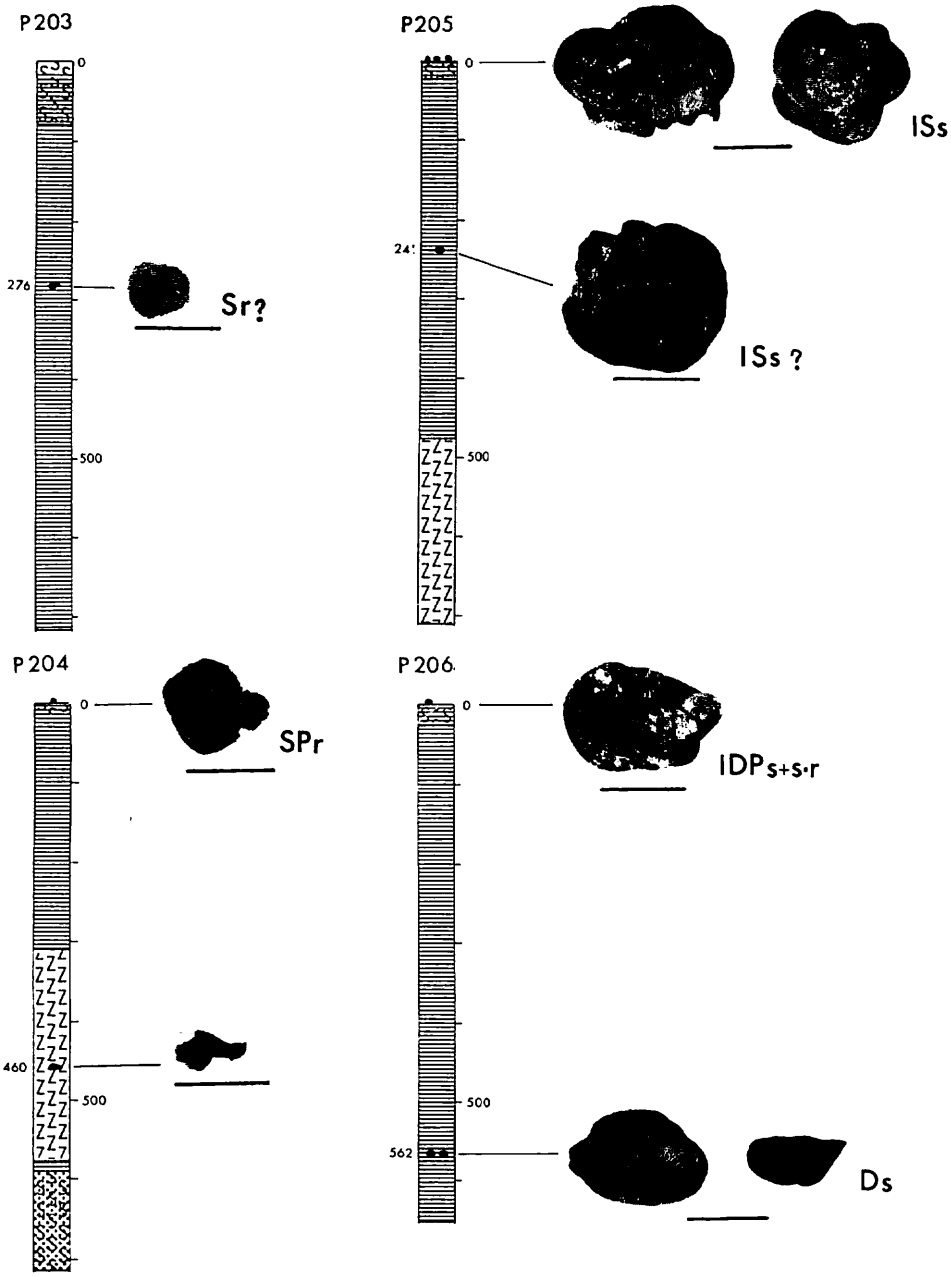

Appendix IX-3 (2)